SVN Stroke & Vascular Neurology

Geometric features of middle cerebral artery are associated with spontaneous basal ganglia intracerebral haemorrhage

Dehan Liu,[1] Guopeng Zhang,[2] Yingliang Wang,[1] Jing Li,[3] Peng Cao,[4] Xiaoxv Yin,[5] Changjun Zhou,[6] Mengdie Wang [7]

To cite: Liu D, Zhang G, Wang Y, *et al*. Geometric features of middle cerebral artery are associated with spontaneous basal ganglia intracerebral haemorrhage. *Stroke & Vascular Neurology* 2022;**0**. doi:10.1136/svn-2021-001277

► Additional supplemental material is published online only. To view, please visit the journal online (http://dx.doi.org/10.1136/svn-2021-001277).

DL and GZ contributed equally.

DL and GZ are joint first authors.

Received 11 August 2021
Accepted 14 December 2021

For numbered affiliations see end of article.

Correspondence to
Professor Mengdie Wang;
wangmengdie@hust.edu.cn

ABSTRACT

Background and purpose Haemodynamics around the middle cerebral artery (MCA) and lenticulostriate arteries is believed to play important roles in the vascular rupture and local haemodynamics is subject to vascular geometry. Nonetheless, the relationship between the geometric features of MCA and spontaneous basal ganglia intracerebral haemorrhage (ICH) has not been investigated. To examine the relationship between the MCA geometric features and spontaneous basal ganglia ICH.

Methods This study was of retrospective and observational nature. The study recruited 158 consecutive hospitalised patients with consecutive CT-confirmed unilateral spontaneous basal ganglia ICH. Clinical data were extracted from electronic medical records, and imaging data were evaluated by two trained radiologists. The MCA-related geometric features were examined and their relationship with spontaneous basal ganglia ICH was analysed. Haemodynamic analyses under different MCA structural features were conducted.

Results Compared with the contralateral MCA, the ipsilateral MCA had greater M1 diameter ratio (proximal/distal) and a smaller M1/M2 angle and MCA bifurcation angle ($p < 0.01$). Imaging study showed differences in the MCA shape in both sides on coronal plane ($p < 0.05$). These MCA features were significantly correlated with the spontaneous ICH in basal ganglia. The greater M1 diameter ratio (proximal/distal), the inferior-oriented M1, the smaller M1/M2 angle and the superior-oriented M1 conditions increased the pressure, from high to low. The greater M1 diameter ratio (proximal/distal) and the inferior-oriented M1 increased the shear stress at the distal end of M1 segment.

Conclusions The geometric features of MCA were significantly related to the spontaneous ICH in basal ganglia. The risk of haemorrhage, from high to low, included the greater M1 diameter ratio (proximal/distal), the inferior-oriented M1 (distal end), the smaller M1/M2 angle and the superior-oriented M1. Mechanistically, these vascular structural features contribute to increased vascular wall pressure and shear stress, which eventually lead to haemorrhage.

INTRODUCTION

Although spontaneous intracerebral haemorrhage (ICH) accounts for less than 20% of cases of stroke, it represents the most serious type of the condition and has the highest mortality among all forms of stroke.[1] Spontaneous ICH in the basal ganglia (the most common site) is caused by the rupture of lenticulostriate arteries (LSAs), the perforating branches of the ipsilateral middle cerebral artery (MCA).[2] As we know it, this region is also a frequent site of ischaemic stroke. Haemorrhagic and ischaemic strokes had some risk factors in common, such as hypertension, diabetes, hyperlipaemia, smoking and alcohol use.[3] In clinical practice, it is still difficult to identify populations who are at higher risk for haemorrhage. Haemodynamics around the MCA and LSAs is believed to play important roles in the vascular rupture and local haemodynamics can be impacted by vascular geometry.[4–8] Previous histological evaluation found that, unlike ischaemic stroke, non-stenotic atherosclerotic MCAs were more common in ICH and it was hypothesised that arterial hypertension spread more easily to the small branches through the main vascular trunks without luminal narrowing, resulting in vascular rupture and haemorrhage.[9] Therefore, we are led to speculate that some geometric features of MCA, which presumably affect both local haemodynamics and wall mechanics, might make the region more vulnerable to spontaneous basal ganglia ICH.

Studies have confirmed that the geometry of intracranial artery is an important factor in the development of atherosclerotic plaque.[10–12] The arterial geometry, by haemodynamically working on the endothelia, can influence the growth of atherosclerotic plaques through the haemodynamic effect, leading to a consistency in geometry among different plaques.[13] Moreover, the geometric properties of plaque can directly influence the risk of plaque rupture.[14 15] In fact, the plaque features, including geometry, are found to be associated with the acute symptoms in MCA.[16] Nonetheless, the haemodynamic mechanisms underlying the plaque formation have not been fully clarified.

In recent years, computational fluid mechanics has emerged as a powerful tool to more precisely explore the cause of cerebral haemorrhage, to probe the mechanism underlying the complex physical events in brain and to serve as a supplement to other medical equipment for higher precision.[17–21] Researchers reportedly simulated the cerebral circulation to look into the pathogenesis of ICH.[22] However, to our knowledge, the relationship between the MCA geometric features and spontaneous basal ganglia ICH have not been investigated, especially by using the computational fluid dynamic (CFD) technique. The objective of this study was, therefore, to examine the MCA geometric features and their effect on the development of spontaneous ICH in basal ganglia by means of CFD simulation. We tried to identify local geometric risk factors that could serve as indicators for identifying populations who are at high risk of spontaneous basal ganglia ICH.

METHODS

Enrolled into this study were the consecutive patients who had CT-confirmed unilateral spontaneous basal ganglia ICH (>18 years) and had received MR angiography (MRA)/CT angiography (CTA) (within 7 days of onset) in Union Hospital, Tongji Medical College, Huazhong University of Science and Technology, Wuhan, China, between 1 September 2013 and 30 June 2019. The flow diagram for patient selection is shown in figure 1. The clinical data of the patients were collected from the institutional medical database. The parameters used in our study included the MCA-related variables and other items that might be related to spontaneous basal ganglia ICH (figure 2). The CFD analysis using the scFLOW module from MSC Cradle was performed to simulate the cerebral blood flow. Statistical analysis was performed by employing Statistical Product and Service Solutions V.12.0 for Windows. Details are given in online supplemental methods.

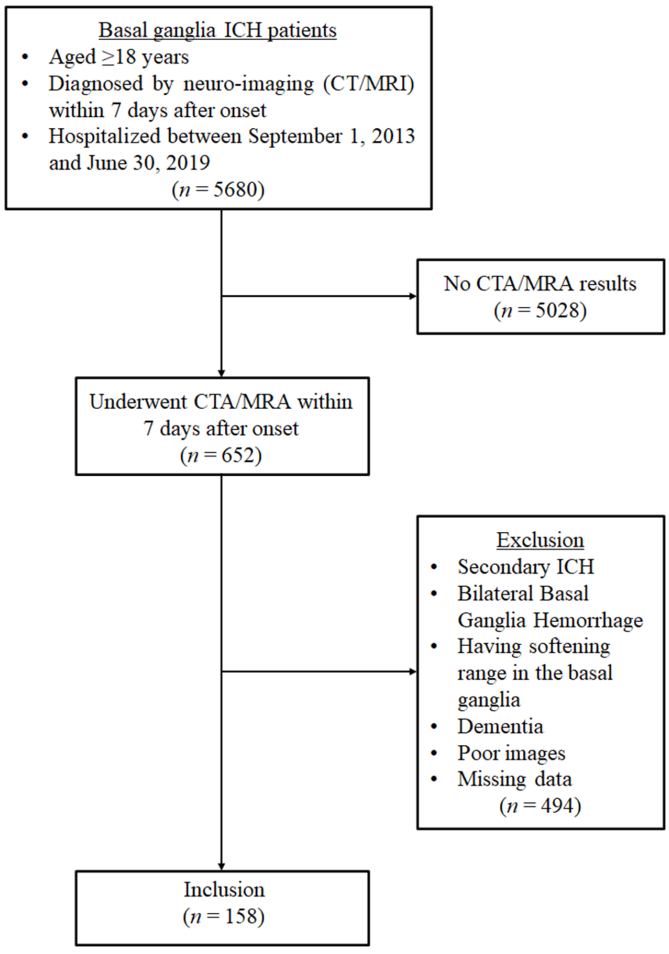

Figure 1 Flow diagram of patient selection. CTA, CT angiography; MRA, MR angiography; ICH, intracerebral haemorrhage.

RESULTS

Basic data

Finally, 158 patients were included in the present analysis. The features of the study population are shown in table 1.

MCA Geometric Features of MCA

The MCA geometric features are summarised in table 2.

Cerebral artery model

The model of human cerebral artery was based on the medical image of human brain CT scan and was generated by three-dimensional reconstruction by using Mimics commercial medical image processing software. The reconstructed model was measured (figure 3). The LSAs divided to branches of four levels (online supplemental figure 2). On the basis of clinical statistical data, models of 5 different lesion MCA geometric features were established (online supplemental figure 3), and then the vascular wall pressure, wall shear stress, and flow rate were observed by employing CFD technology.

Arterial wall pressure distribution

The cloud diagram of the arterial wall pressure distribution and pressure values on the axis of the arterial wall are shown in figure 4A,B. The pressure gradient generally decreased along the flow direction. The highest pressure was about 19.7 kPa at the blood inlet of the proximal end of M1. In the model 1, the wall pressures of M1 and all the level-1 branches of 6 LSAs were marginally higher than that of the basal condition. In the Model 2, the wall pressure at the proximal end of the M1 was relatively high while the distal wall pressure was relatively low. The pressures of the E and F branches (levels 1–3) and at openings of the B and D branches of the LSAs were also elevated. In the Model 3, the pressure, being the highest in all conditions, obviously increased in the M1 and all the level 1–3 branches of 6 LSAs, as compared with other conditions. In the Model 4, the wall pressure was high in the proximal end and dropped at the distant end. The pressure was elevated in all the level 1–2 branches of 6 LSAs and decreased along the flow direction. In the model 5, the

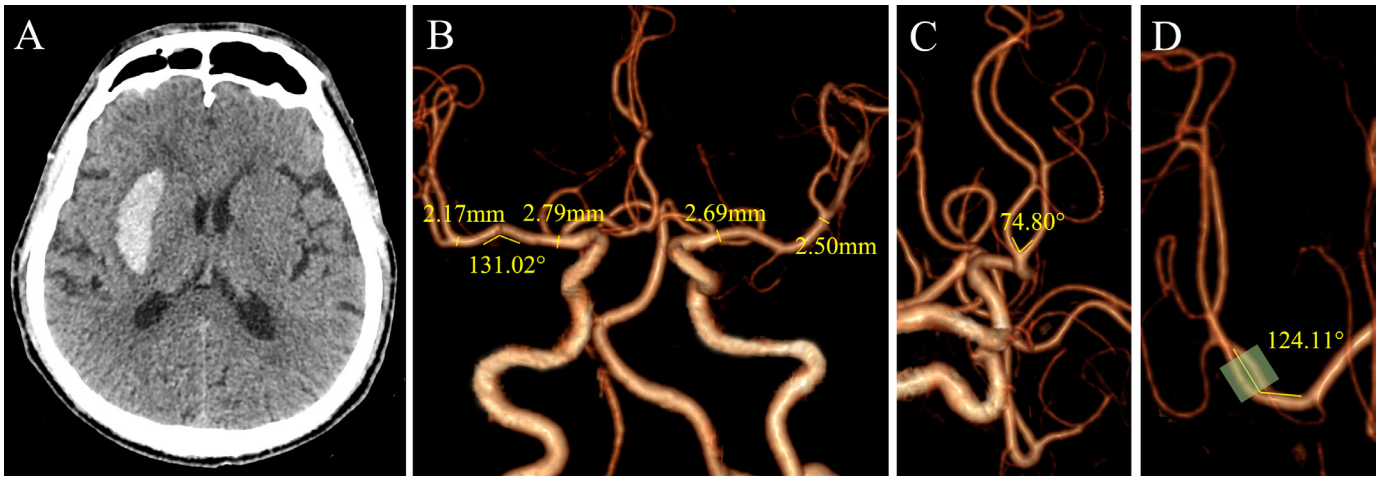

Figure 2 A right spontaneous basal ganglia ICH (A) and measurement of the M1 length (B), M1 proximal/distal diameter (B), M1 curve orientation (B), MCA bifurcation angle (C) and M1/M2 angle (D). ICH, intracerebral haemorrhage; MCA, middle cerebral artery.

Table 1 Clinical characteristics of patients with spontaneous basal ganglia ICH (N=158)

Covariate	No (%)
Age, mean±SD	53.5±10.6
Female	52 (32.9)
Smoking	42 (36.8)
Drinking	33 (29.0)
Hypertension	99 (62.7)
Diabetes mellitus	9 (5.7)
Hypercholesterolaemia	14 (8.9)
Coronary artery disease	4 (2.5)
Previous ICH	3 (1.9)
Previous ischaemic stroke	6 (3.8)
Antihypertensive treatment	25 (15.8)
Antiplatelet treatment	3 (1.9)
Hypoglycaemic treatment	2 (1.3)
Statin treatment	5 (3.2)
Admission BP, mean±SD, mm Hg	
Systolic	149.0±21.5
Diastolic	92.0±16.2
Intraventricular extension	48 (30.4)
M1 segment stenosis	3 (1.9)
Non-responsible aneurysm	4 (2.5)
Anterior cerebral artery predominance	
Lateral	4 (2.5)
Contralateral	9 (5.7)
Treatment	
Conservative	118 (74.7)
Surgical	40 (25.3)
Volume, median (IQR), mL	15.3 (5.4–32.0)

BP, blood pressure; ICH, intracerebral haemorrhage.

working condition exerted little effect on the wall pressure.

Model 3 had the highest pressure, followed by model 2 (distal pattern), model 4 and model 1. The pressure gradients in the centre of base, model 1, model 4 and model 5 were relatively gentle. The pressure did not fluctuate significantly at the M1, but only decreased at the blood inlet and the distal end of M1 segment. The pressure dropped by 0.35–0.4 kPa. In the model 2, the pressure at the centre of the vessel fluctuated substantially. And there was a long low pressure area at the distal end of the M1 segment.

Arterial wall shear stress distribution

The distribution of the arterial wall shear stress under the six working conditions is shown in figure 4C. The distribution was more complicated, with the wall shear stress ranging from 1 to 50 Pa. There was a low shear stress area at the bottom of the level-1 branches of LSAs. The lower shear stress area at the upper arch of the M1 was larger in the model 1 than in the basal condition. In the model 2, there was a large shear stress (45–50 Pa) area at the distal end of M1 and the A and B branch opening of the LSAs also increased. In the model 3, the shear stress at the distal end of M1 increased and so did the B and C branch opening of the LSAs. In the model 4, the shear stress rose at the distal pattern of M1. Compared with the basal condition, the shear stress distribution of model 5 was essentially the same.

DISCUSSION

In this study, a rationale was addressed on the association between the MCA geometric features and spontaneous basal ganglia ICH, by using numerical simulation. Our results showed that, the MCA geometric features, in terms of M1 diameter ratio (proximal/distal), M1 curve orientation on coronal image plane, and M1/M2 angle, were significantly related to the spontaneous ICH in basal

Table 2 MCA geometric features (N=158)

Covariate	Ipsilateral side	Contralateral side	P value
M1 length, mean±SD, mm	19.3±6.8	18.2±6.8	0.0534
M1 proximal diameter, mean±SD, mm	2.3±0.4	2.3±0.4	0.6127
M1 distal diameter, mean±SD, mm	1.9±0.4	2.1±0.4	<0.0001
M1 diameter ratio (proximal/ distal), mean±SD	1.2±0.2	1.1±0.1	<0.0001
M1 shape and curve orientation (axial), N (%)			0.1814
Dorsal	79 (50.0)	93 (58.9)	
Ventral	35 (22.1)	22 (13.9)	
Straight	36 (22.8)	38 (24.0)	
Sigmate	8 (5.1)	5 (3.2)	
Bending angle (axial), mean±SD	154.4±18.4	155.6±17.8	0.4167
M1 shape and curve orientation (coronal), N (%)			0.0414
Superior	85 (53.8)	91 (57.6)	
Inferior	48 (30.4)	28 (17.7)	
Straight	16 (10.1)	31 (19.6)	
Sigmate	9 (5.7)	8 (5.1)	
Bending angle (coronal), mean±SD	148.0±21.0	152.2±20.0	0.0500
M1/M2 angle, mean±SD	128.3±23.4	134.0±24.3	0.0074
MCA bifurcation angle, mean±SD	80.3±25.1	94.4±25.6	<0.0001

ganglia. The factors that increase the risk of haemorrhage, from high to low, include the greater M1 diameter ratio (proximal/distal), the inferior-oriented M1 (distal end), the smaller M1/M2 angle, and the superior-oriented M1 segment. Our results suggested that these vascular structural features contribute to the increased arterial wall pressure and shear stress, which may pathologically underlie the development of haemorrhage.

Vascular geometry has been suggested as a factor that regulates haemodynamics and consequently influences the development of vascular diseases, such as atherosclerosis and cerebral aneurysmal disease, in which blood exerts excessive forces on the vascular wall.[23 24] In reality, the vascular anatomy varies substantially. Some geometric features may be 'geometric risk factors' that bring about high haemodynamic shear stresses on the local vascular wall.[25] Like the aforementioned diseases, spontaneous ICH is also presumed to be related to the geometry of intracranial vessels. Zhang *et al*[22] found that the angle between the MCA and the internal carotid artery and the distance between the beginning of the median artery and superior trunk were significantly related to ICH. Lee *et al*[7] also reported that putaminal ICH occurred more frequently on the side of the dominant anterior cerebral artery first segment. These might be ascribed to local haemodynamic changes caused by certain geometrical variations, but the assumption still awaits further confirmation.

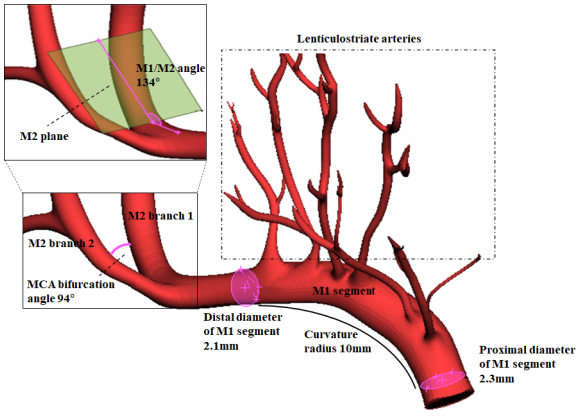

Figure 3 Primary cerebral artery model and measurement of the MCA-related geometric features. MCA, middle cerebral artery.

Most spontaneous ICHs occurs in the basal ganglia, resulting from the rupture of the LSAs which bear more wall pressure or shear stress.[26 27] LSAs are small branches of the MCA and the main perforators supplying basal ganglia.[4] Therefore, the haemodynamics of LSAs is presumably affected by the MCA. Technically, direct measurement of the pressure or sheer stress of intracranial arteries remains a significant challenge in clinical practice. However, measuring the geometry of intracranial arteries is convenient, given the wide application of noninvasive vascular imaging, such as MRA and CTA. LSAs cannot be well visualised by MRA/CTA. Therefore, we focused on the MCA, with an attempt to find some geometric features that help predict the risk for ICH taking place in this deep brain area without obtaining local haemodynamic data.

In this study, a set of geometric features, presumed to impact the MCA haemodynamics, were then selected and measured. We found that, unlike ischaemic stroke, atherosclerotic plaque and stenosis at M1 segment were rare, which is consistent with the findings of an autopsy

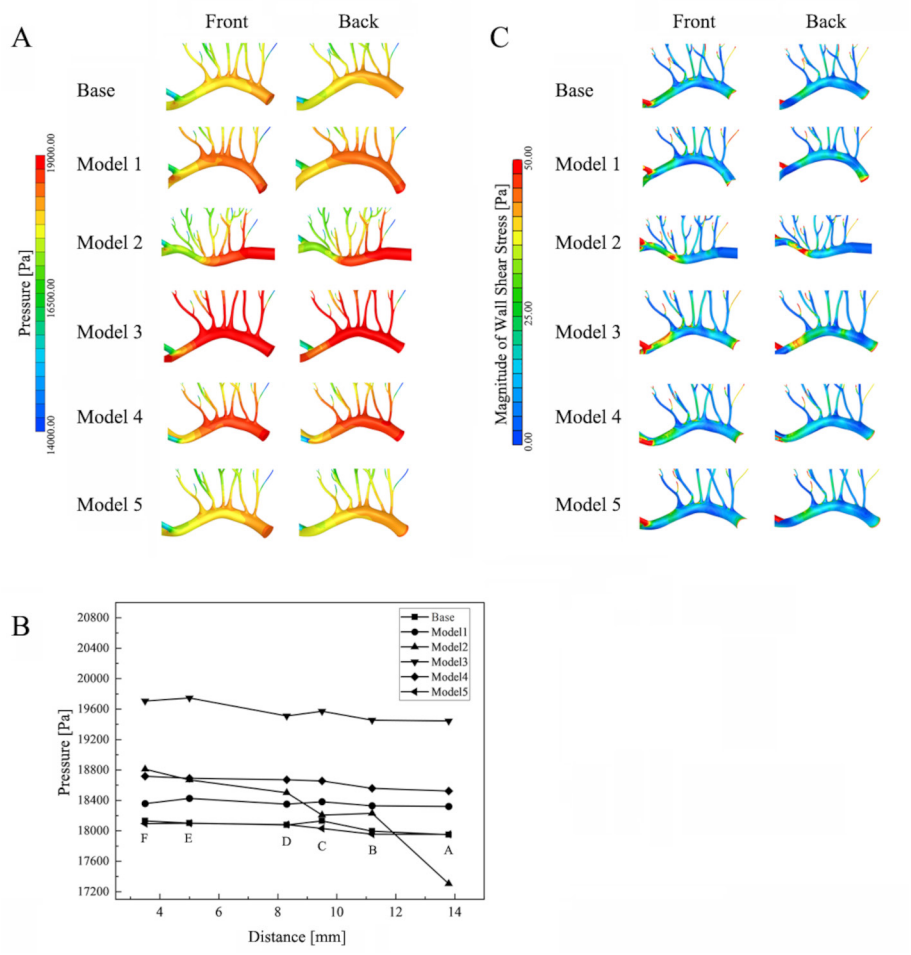

Figure 4 Haemodynamics analyses. (A) Arterial wall pressure distribution nephogram. (B) Arterial wall pressure distribution diagram. (C) Arterial wall shear stress distribution cloud chart.

study.[9] As with healthy population,[28] curved MCAs were more prevalent than their straight counterparts. The dorsal and superior-oriented M1 segment curves were found to be the most common shape of MCAs in our study. This curve orientation is just opposite to that observed in a previous study on atherosclerotic MCAs,[11] and this disparity might be attributed to the difference in subjects selection between the two studies. But the proportion of the curved M1 segment and inferior-oriented M1 segment curves were higher in the haemorrhage side. Further analysis showed that M1 diameter ratio (proximal/distal), M1 curve orientation on coronal image plane, M1/M2 angle and MCA bifurcation angle were independently associated with basal ganglia ICH. However, no correlations were found between these geometric features and haematoma volume (online supplemental table 1) or severity (online supplemental table 2), respectively.

A question presents itself: Whether these MCA structural features may raise local haemodynamic stresses and further result in haemorrhage? Further haemodynamic analyses revealed that the greater M1 diameter ratio (proximal/distal), the inferior-oriented M1 (distal end), the smaller M1/M2 angle and the superior-oriented M1, from high to low, could significantly increase M1 segment and LSAs wall pressure. The wall pressure gradient generally decreased along the flow direction under all these conditions. The elevated wall pressure of LSAs might lead to vascular rupture and haemorrhage in the condition that the brain pressure increases due to some unexpected stimulation. With greater M1 diameter ratio (proximal/distal), the wall pressure of all the level 1–3 branches of 6 LSAs were significantly elevated, rendering the areas prone to rupture. With smaller M1/M2 angle and superior-orientation of M1, the rupture-prone zones were at all the level-1 branches of six LSAs. Inconsistent with the aforementioned conditions, the inferior-orientation of M1 substantially increased the pressure of the proximal LSA branches. The rupture-prone zones were at the E and F branches (levels 1–3) and openings of the B and D branches. The role of the low pressure aera formed at the distal end of M1 warrants further study, and some unknown factors might contribute to the vascular rupture. Moreover, the wall shear stress under the four conditions ranged from 1 to 50 Pa. This might explain why M1 segment atherosclerotic plaques and segmental stenosis are rare in ICH patients since atherosclerotic plaques usually develop in areas where the wall shear stress is lower than 0.1 Pa.[23] With greater M1 diameter

ratio (proximal/distal) and the inferior-orientation of M1, the shear stress at the distal end of M1 segment was greatly increased, leading by a high blood velocity. The high wall shear stress has a greater scouring force on the inner wall of the vascular, causing damage to the endothelial cells of the vessels. This might increase the risk of distal LSAs rupture and haemorrhage. Furthermore, it is worth noting that curve orientation and curvature were two important factors that are associated with the risk of haemorrhage when M1 is curved. The inferior-oriented M1 segment is more susceptible to haemorrhage more than the superior-oriented one. We are led to conclude that the greater the positive curvature, the higher the pressure, and the smaller the distal shear stress. On the contrary, the smaller the negative curvature, the higher the pressure, and the greater the distal shear stress. Therefore, these four MCA structural features statistically suffice to cause basal ganglia ICH by increasing the arterial wall pressure and shear stress. The risk of haemorrhage, from high to low, included the greater M1 diameter ratio (proximal/distal), the inferior-oriented M1, the smaller M1/M2 angle and the superior-oriented M1 segment.

Our study had some limitations. First, the MCA geometric features selected in the study might not cover all parameters that affect local haemodynamics. Other geometric parameters, such as wall thickness, might also be important determinants, but these data are not available from the MRA/CTA images. Second, LSAs, which are subject to structural variation and sufficient to impact local haemodynamics, were not covered by this study since they could not be visualised by MRA/CTA. Third, this study was retrospective, single-centred and self-controlled nature. Further prospective multisetting studies in larger populations are needed.

Summary

In conclusion, our results are potentially of clinical importance. We confirmed that geometric risk factors were at work in the development of basal ganglia ICH. Some MCA geometric features, such as greater M1 diameter ratio (proximal/distal), curved M1 on coronal image plane, and smaller M1/M2 angle, were indicative of high risk of ICH in this deep brain area without support of local haemodynamic data. Identification of these risk features of the MCA might greatly facilitate the control and prevention of ICH in basal ganglia.

Author affiliations
[1]Department of Radiology, Union Hospital, Tongji Medical College of Huazhong University of Science and Technology, Wuhan, Hubei, China
[2]Department of Nuclear Medicine, Tongji Hospital, Tongji Medical College of Huazhong University of Science and Technology, Wuhan, Hubei, China
[3]MSC CFD Cradle BD, MSC oftware Corporation, Shanghai, China
[4]Faculty of Architecture, Civil and transportation Engineering, Beijing University of Technology, Beijing, China
[5]School of Public Health, Tongji Medical College of Huazhong University of Science and Technology, Wuhan, Hubei, China
[6]School of Transportation and Logistics, Dalian University of Technology, Dalian, Liaoning, China
[7]Department of Neurology, Union Hospital, Tongji Medical College of Huazhong University of Science and Technology, Wuhan, Hubei, China

Correction notice This article has been corrected since published online first. DL and GZ contributed equally and are joint first authors.

Contributors MW are responsible for the overall content as the guarantor. Concept and design: MW; acquisition, analysis or interpretation of data: MW, DL, GZ, YW, JL, PC, XY; drafting of the manuscript: MW, DL, GZ, YW, PC, XY, CZ; critical revision of the manuscript for important intellectual content: MW; statistical analysis: JL, PC, XY; obtained funding: MW; administrative, technical or material support: MW, DL, GZ, YW, JL, PC and XY; supervision: MW.

Funding This work was supported by grants from the Program of National Natural Science Foundation of China (81301001, 81301248, 81801181).

Competing interests None declared.

Patient consent for publication Not applicable.

Provenance and peer review Not commissioned; externally peer reviewed.

Data availability statement Data are available on reasonable request. All free text entered below will be published.

ORCID iD
Mengdie Wang http://orcid.org/0000-0001-6181-0697

REFERENCES

1 Gross BA, Jankowitz BT, Friedlander RM. Cerebral intraparenchymal hemorrhage: a review. *JAMA* 2019;321:1295.
2 Greenberg SM. Small vessels, big problems. *The New England Journal of Medicine* 2016.
3 Li Q, Huang Y-J, Zhang G, *et al*. Intraventricular hemorrhage and early hematoma expansion in patients with intracerebral hemorrhage. *Sci Rep* 2015;5.
4 Hu R, Feng H. Lenticulostriate artery and lenticulostriate-artery neural complex: new concept for intracerebral hemorrhage. *Curr Pharm Des* 2017;23:2206–11.
5 Qureshi AI. The importance of acute hypertensive response in ICH. *Stroke* 2013;44:S67-9.
6 Oeinck M, Neunhoeffer F, Buttler K-J, *et al*. Dynamic cerebral autoregulation in acute intracerebral hemorrhage. *Stroke* 2013;44:2722–8.
7 Lee J-H, Chang C-H, Jung Y-J, *et al*. The relationship between the direction of putaminal intracerebral hemorrhage and anterior cerebral artery predominance. *World Neurosurg* 2017;107:211–5.
8 Piccinelli M, Veneziani A, Steinman DA, *et al*. A framework for geometric analysis of vascular structures: application to cerebral aneurysms. *IEEE Trans Med Imaging* 2009;28:1141–55.
9 Araki G, Mihara H, Mizukami M, *et al*. Comparative angiographic and histological evaluations of intracranial atherosclerosis in hypertensive and normotensive subjects. *Stroke* 1978;9:364–8.
10 Kim BJ, Kim SM, Kang D-W, *et al*. Vascular tortuosity may be related to intracranial artery atherosclerosis. *Int J Stroke* 2015;10:1081–6.
11 Yu YN, Li M-L, Xu Y-Y, *et al*. Middle cerebral artery geometric features are associated with plaque distribution and stroke. *Neurology* 2018;91:e1760–9.
12 Lan L, Liu H, Ip V, *et al*. Regional high wall shear stress associated with stenosis regression in symptomatic intracranial atherosclerotic disease. *Stroke* 2020;51:3064–73.
13 Liu H, Wingert A, Wang X, *et al*. Consistency in geometry among coronary atherosclerotic plaques extracted from computed tomography angiography. *Front Physiol* 2021;12:715265.
14 Choi G, Lee JM, Kim H-J, *et al*. Coronary artery axial plaque stress and its relationship with lesion geometry: application of computational fluid dynamics to coronary CT angiography. *JACC Cardiovasc Imaging* 2015;8:1156–66.
15 Liu H, Leung T, Wong A. The geometric effects on the stress of arterial atherosclerotic plaques: a computational study. *Annual International Conference of the IEEE engineering in medicine and biology Society. IEEE Engineering in Medicine and Biology Society. Annual International Conference*, 2019.

16 Li S, Song X, Hu Q, *et al*. Association of plaque features with infarct patterns in patients with acutely symptomatic middle cerebral artery atherosclerotic disease. *J Stroke Cerebrovasc Dis* 2021;30:105724.
17 Mori F, Ishida F, Natori T, *et al*. Computational fluid dynamics analysis of lateral striate arteries in acute ischemic stroke using 7T high-resolution magnetic resonance angiography. *J Stroke Cerebrovasc Dis* 2019;28:104339.
18 Chen Z, Qin H, Liu J, *et al*. Characteristics of wall shear stress and pressure of intracranial atherosclerosis analyzed by a computational fluid dynamics model: a pilot study. *Front Neurol* 2019;10:1372.
19 Liu H, Lan L, Abrigo J. Comparison of newtonian and non-newtonian fluid models in blood flow simulation in intracranial atherosclerotic stenosis. *Frontiers in Physiology* 2021.
20 Saqr KM, Mansour O, Tupin S, *et al*. Evidence for non-newtonian behavior of intracranial blood flow from doppler ultrasonography measurements. *Med Biol Eng Comput* 2019;57:1029–36.
21 Liu H, Wang D, Leng X. State-of-the-art computational models of circle of Willis with physiological applications: a review. *IEEE* 2020.
22 Zhang L, Li J, Yin K, *et al*. Computed tomography angiography-based analysis of high-risk intracerebral haemorrhage patients by employing a mathematical model. *BMC Bioinformatics* 2019;20:193.
23 Malek AM, Alper SL, Izumo S. Hemodynamic shear stress and its role in atherosclerosis. *JAMA* 1999;282:2035.
24 Hoi Y, Meng H, Woodward SH, *et al*. Effects of arterial geometry on aneurysm growth: three-dimensional computational fluid dynamics study. *J Neurosurg* 2004;101:676–81.
25 Friedman MH. Variability of 3D arterial geometry and dynamics, and its pathologic implications. *Biorheology* 2001.
26 Chien S, Li S, Shyy YJ. Effects of mechanical forces on signal transduction and gene expression in endothelial cells. *Hypertension* 1998;31:162–9.
27 Chiu J-J, Chien S. Effects of disturbed flow on vascular endothelium: pathophysiological basis and clinical perspectives. *Physiol Rev* 2011;91:327–87.
28 Han J, Qiao H, Li X, *et al*. The three-dimensional shape analysis of the M1 segment of the middle cerebral artery using MRA at 3T. *Neuroradiology* 2014;56:995–1005.

SUPPLEMENTAL MATERIAL

STROBE Statement-Checklist

	No.	Recommendation	
Title and abstract	1	(a) indicate the study's design with a commonly used term in the title or the abstract	P1L10
		(b) Provide in the abstract an informative and balanced summary of what was done and what was found	P1-2
Introduction			
Background/rationale	2	Explain the scientific background and rationale for the investigation being reported.	P3L2-P4L2
Objective	3	State specific objectives, including any prespecified hypotheses	P4L5-9
Methods			
Study design	4	Present key elements of study design early in the paper	P4L11-19
Setting	5	Describe the setting, locations, and relevant dates, including periods of recruitment, exposure, follow-up, and data collection	P4L11-19
Participants	6	*(a)* Give the eligibility criteria, and the sources and methods of selection of participants	supplemental material P4L3-11
Variables	7	Clearly define all outcomes, exposures, predictors, potential confounders, and effect modifiers. Give diagnostic criteria, if applicable	P4L11-14
Data sources/ measurement	8	For each variable of interest, give sources of data and details of methods of assessment (measurement). Describe comparability of assessment methods if there is more than one group	supplemental material P5L5-P8L13
Bias	9	Describe any efforts to address potential sources of bias	N/A
Study size	10	Explain how the study size arrived at	supplemental material P4L3-11
Quantitative variables	11	Explain how quantitative variables were handled in the analyses. If applicable, describe which grouping were chosen and why	N/A
Statistical methods	12	(*a*) Describe all statistical methods, including those used to control for confounding	supplemental material P8L15-P9L10
		(*b*) Describe any methods used to examine subgroups	N/A

		and interactions	
		(*c*) Explain how missing data were addressed	supplemental material P4L10-11
		(*d*) If applicable, describe analytical methods taking account of sampling strategy	N/A
		(*e*) Describe any sensitivity analyses	N/A
Results			
Participants	13	(*a*) Report numbers of individuals at each stage of study – e.g. numbers potentially eligible, examined for eligibility, confirmed eligible, included in the study, completing follow-up, and analysed	P5L3
		(*b*) Give reasons for non-participation at each stage	N/A
		(*c*) Consider use of a flow diagram	P4L16
Descriptive data	14	(*a*) Give characteristics of study participants (e.g. demographic, clinical, social) and information on exposures and potential confounders	P5L3-4
		(*b*) Indicate number of participants with missing data for each variable of interest	supplemental material P4L10-11
Outcome data	15*	Report numbers of outcome events or summary measures	N/A
Main results	16	(*a*) Give unadjusted estimates and, if applicable, confounder-adjusted estimates and their precision (e.g. 95% confidence interval). Make clear which confounders were adjusted for and why they were included	N/A
		(*b*) Report category boundaries when continuous variables were categorized	N/A
		(*c*) If relevant, consider translating estimats of relative risk into absolute risk for a meaningful time period	N/A
Other analyses	17	Report other analyses done – e.g. analyses of subgroups and interactions, and sensitivity analyses	N/A
Discussion			
Key results	18	Summarise key results with reference to study objectives	P9L21-P10L8
Limitation	19	Discuss limitations of the study, taking into account sources of potential bias or imprecision. Discuss both direction and magnitude of any potential bias	P13L18-P14L3
Interpretation	20	Give a cautious overall interpretation of results considering objectives, limitations, multiplicity of analyses, results from similar studies, and other relevant evidence	P11L11-P13L17

Generalisability	21	Discuss the generalisability (external validity) of the study resultes	P14L1-3
Other information			
Funding	22	Give the source of founding and the role of the founders for the present study and, if applicable, for the original study on which the present article is based	P14L13-14

Supplemental Methods

Participants

Enrolled into this study were the consecutive patients who had CT-confirmed unilateral spontaneous basal ganglia ICH (> 18 years) and had received magnetic resonance angiography (MRA)/computed tomography angiography (CTA) (within 7 days of onset) in Union Hospital, Tongji Medical College, Huazhong University of Science and Technology, Wuhan, China, between September 1, 2013 and June 30, 2019. The clinical data of the patients were collected from the institutional medical database. Those who had secondary ICH, softening range in the basal ganglia, dementia, no M1 segment, and poor imaging data were excluded. Patients whose data were missing or not available were also eliminated. The flow diagram for patient selection is shown in Figure 1. All patients' MRA/CTA images were analyzed from the ipsilateral side, with the contralateral side serving as a self-control, to study the high-risk features of ICH. The requirement for informed consent from patients was waived by the ethics committee due to the retrospective nature of the study. The data are anonymous, and all authors could only use the anonymized data for statistical analysis. STROBE was used as the reporting guideline and no extensions were used.

Neuroimaging Data

MRI was performed on a 3.0-tesla system (SIEMEHS) equipped with adequate head coils. The protocol included conventional 3-dimensional time-off light MRA, T1-weighted imaging, and T2-weighted imaging of the head. Maximum intensity projection (MIP) images were reconstructed from 3-dimensional time-off light MRA

on axial, sagittal and coronal planes in all patients. CT was performed on a 64-slice system (PHILIPS-CX). The protocol involved conventional CTA and plain CT scan of the head. MIP images were reconstructed from CTA on axial, sagittal and coronal planes in all patients.

The parameters used in our study included the MCA-related variables and other items that might be related to spontaneous basal ganglia ICH. All the parameters were measured on the Picture Archiving and Communication System. The MCA-related geometric features examined included M1 length, M1 proximal/distal diameter, shape of M1, M1 curve orientation, M1/M2 angle and MCA bifurcation angle (Figure 2A-D). M1 length and proximal/distal diameter were measured on axial plane. Shape of M1 was categorized as straight or curved based on axial and coronal MIP images of 3-dimensional time-off light MRA/CTA. We determined the orientation of the curved M1 on the basis of the direction(s) in which each M1 curve opened and measured the angle in the two directions respectively. Ventral- and dorsal-oriented M1 curves were identified by using axial MIP images, while superior- and inferior-oriented M1 curves were identified using coronal MIP images. The M1/M2 angle (the angle between M1 segment and the plane where the M2 branches were on) and MCA bifurcation angle (the angle of two M2 branches; all have two branches in our cases) were measured in different directions to fully present the relative position among the vessels. Windowing for the 3D reconstructions was validated against the multiplanar reconstructions to ensure accurate measurement.

Other parameters included the hematoma volume, and presence (or absence) of

intraventricular extension, aneurysm(s) in the adjacent vessels and stenosis of the M1 segment. The hematoma volume was measured in Picture Archiving and Communication System. The researcher manually outlined the hematoma and then the system calculated the volume automatically.

Images were analyzed twice by a researcher who was blind to all clinical information, with the two analyses being 1 month apart. To evaluate the consistency between examiners, another image reader, also blind to all clinical data, assessed 50 imaging materials randomly and independently selected from the overall imaging materials.

Control Equation of the Blood Flow in the Cerebral Vessels

Hemodynamically, the Naviers-Stokes equation, continuity equation, and motion equation of incompressible viscous fluids are commonly used to describe blood flow. The basic mechanical laws of viscous fluid flow are described, and the formulae were as follows:

(1) Naviers-Stokes equation

$$\frac{\partial v}{\partial t} + (v \bullet \Delta)v = -\frac{1}{\rho}\Delta p + \frac{\eta}{p}\Delta^2 v$$

where, v represents fluid velocity, ρ fluid density, p pressure, and η hemodynamic viscosity.

(2) Continuity equation

$$\frac{\partial u}{\partial x} + \frac{\partial v}{\partial y} + \frac{\partial w}{\partial z} = 0$$

where *u*, *v*, and *w* are the velocity components of the velocity vector on *x*, *y*, and *z*, respectively.

(3) Momentum conservation equation

$$\frac{\partial(\rho u)}{\partial t}+div(\rho uU)=div(\eta gradu)+Su-\frac{\partial p}{\partial x}$$
$$\frac{\partial(\rho v)}{\partial t}+div(\rho vU)=div(\eta gradv)+Sv-\frac{\partial p}{\partial y}$$
$$\frac{\partial(\rho w)}{\partial t}+div(\rho wU)=div(\eta gradw)+Sw-\frac{\partial p}{\partial z}$$

where, *u*, *v,* and *w* are the velocity components of the velocity vector on *x*, *y,* and *z*, respectively, and η is the dynamic viscosity of the fluid; *Su*, *Sv,* and *Sw* are the broad source terms of the three momentum conservation equations, respectively.

(4) Fluid properties

In the study, blood was seen as an incompressible Newtonian fluid, with blood density ρ=1050 kg/m^3 and viscosity=0.0024 Pa·s (in ref 10, the viscosity was set at 0.0035, being virtually identical to the parameter used in the present paper). This study ignored the influence of gravity in the simulation, and the vascular wall was taken as a non-viscoelastic rigid wall under the condition of no slip referring to the previous studies. [1-3] The inner diameter at the entrance of M1 segment was within 2.1~2.7 mm. We enrolled 158 patients, the peak blood velocity in the brain was 0.4~1.1 m/s, and the peak Re of Re=$\rho vD/\mu$ number was 367~1300. Therefore, in the numerical simulation, the blood movement in the cerebral artery was assumed to be a steady laminar flow, and the inlet flow rate was defined as 5e-6 m^3/*s*.

(5) Geometric model, mesh and boundary conditions

In the analysis with the scFLOW module from MSC Cradle, the grid was first divided based on the scFLOW Preprocessor software. Due to the irregularity and complexity of the model, the unstructured octree method was adopted to divide it, and the grid was of polyhedral type. The meshes were divided into intelligent meshes, i.e., when the geometric shapes change, the meshes divided automatically and reasonably according to the geometric shapes encountered, so as to obtain a relatively optimal mesh cell. For MCA meshing, non-equidistant meshing along the radius direction was adopted to improve the calculation accuracy of the boundary layer of the pipe wall, while for all LSAs, non-equidistant meshing was used and local refinement was performed at each bifurcation point to improve the accuracy. There were roughly 1.35 million units in the model (supplementary Figure 1), and the convergence is also provided and discussed in this paper. Furthermore, the mesh data including the boundary layer zone, are also detailed in supplementary Figure 5.

Statistical analysis

Statistical analysis was performed by employing Statistical Product and Service Solutions 12.0 for Windows. For descriptive analysis, frequency and percentage were used for independent variables. The paired *t*-test was employed to compare quantitative data of the MCA geometric features. The Bowker test was utilized to compare enumeration data of the MCA geometric features. Then, multivariate logistic regression analysis was conducted to identify the association between the MCA geometric features and hematoma volume. Variables input into the model included age, gender, smoking and drinking habits, hypertension, diabetes mellitus,

hypercholesterolemia, coronary artery disease, previous ischemic stroke, previous ICH, time of scanning, intraventricular extension and the geometric features of MCA. The relationship between the MCA geometric features and NIHSS score was also examined by multivariate logistic regression. Variables input into the model were age, gender, smoking and drinking habits, hypertension, diabetes mellitus, hypercholesterolemia, coronary artery disease, previous ischemic stroke, previous ICH, time of scanning, intraventricular extension, hematoma volume and the MCA geometric features. Adjusted odds ratios (ORs) and 95% confidence intervals (CIs) for variables were obtained. For all analyses, differences were tested using two-tailed tests, and a $P<0.05$ was considered to be statistically significant.

Supplemental references

1. Leng X, Lan L, Ip HL, et al. Hemodynamics and stroke risk in intracranial atherosclerotic disease. Ann Neurol. 2019 May;85(5):752-764.
2. Leng X, Scalzo F, Ip HL, et al. Computational fluid dynamics modeling of symptomatic intracranial atherosclerosis may predict risk of stroke recurrence. PLoS One. 2014 May 12;9(5):e97531.
3. Liu J, Yan Z, Pu Y, et al. Functional assessment of cerebral artery stenosis: a pilot study based on computational fluid dynamics. J Cereb Blood Flow Metab. 2017 Jul;37(7):2567-2576.

Supplemental Tables

Table 1 shows determinants associated with hematoma volume. Patients who had suffered hypertension had larger hematoma volume (β=9.83, SE=4.93, *P*=0.0492), while patients who had intraventricular extension had smaller hematoma volume (β=-13.22, SE=3.80, P=0.0008). Other covariates, including MCA geometric features, showed no significant differences in multivariable linear regression analysis.

Covariate	**Intracerebral Hemorrhage Volume**	
	β (SE)	***P* Value**
Age	-0.18 (0.17)	0.3143
Gender	-1.11 (4.45)	0.8045
Smoking	-0.27 (4.60)	0.9539
Drinking	-1.58 (4.40)	0.7208
Hypertension	9.83 (4.93)	0.0492
Diabetes mellitus	6.81 (7.44)	0.3625
Hypercholesterolemia	0.97 (5.21)	0.8523
Coronary artery disease	-6.96 (9.21)	0.4519
Previous ischemic stroke	7.77 (7.52)	0.3044
Previous ICH	15.88 (10.78)	0.1444
Time to scan	0.14 (0.11)	0.2153
Intraventricular extension	-13.22 (3.80)	0.0008
M1 length	0.42 (0.30)	0.1572
M1 diameter ratio (proximal/ distal)	-14.54 (8.85)	0.1041

M1 shape and curve orientation (axial)	-3.45 (6.46)	0.5952
Bending angle (axial)	0.01 (0.18)	0.9347
M1 shape and curve orientation (coronal)	-2.16 (6.61)	0.7446
Bending angle (coronal)	0.16 (0.09)	0.0886
M1/M2 angle	0.02 (0.08)	0.8276
MCA bifurcation angle	-0.06 (0.07)	0.4325

Table 2 shows determinants associated with NIHSS score. Predictors of NIHSS score identified through multivariable linear regression analysis were age and hematoma volume. The older patients (β=0.27, SE=0.11, *P*=0.0161) and those who had larger hematoma volume (β=0.26, SE=0.06, *P*=0.0002) had higher NIHSS score. Other covariates, including MCA geometric features, were not associated with NIHSS score.

Covariate	**NIHSS score**	
	β (SE)	***P* Value**
Age	0.27 (0.11)	0.0161
Gender	2.29 (2.87)	0.4269
Smoking	1.97 (2.72)	0.4721
Drinking	-0.60 (2.72)	0.8278
Hypertension	0.80 (3.20)	0.8023
Diabetes mellitus	4.67 (4.69)	0.3241
Hypercholesterolemia	2.85 (3.07)	0.3570
Coronary artery disease	-3.72 (5.90)	0.5312
Previous ischemic stroke	4.01 (5.13)	0.4380
Previous ICH	2.72 (11.47)	0.8133
Time to scan	0.09 (0.21)	0.6527
Intraventricular extension	-4.72 (2.39)	0.0528
Hematoma volume	0.26 (0.06)	0.0002
M1 segment length	-0.16 (0.21)	0.4485

M1 segment diameter ratio (proximal/ distal)	3.76 (5.39)	0.4886
M1 segment shape and curve orientation (axial)	2.88 (4.04)	0.4785
Bending angle (axial)	-0.07 (0.12)	0.5756
M1 segment shape and curve orientation (coronal)	1.62 (3.74)	0.6659
Bending angle (coronal)	0.08 (0.06)	0.2090
M1/M2 angle	-0.03 (0.05)	0.5760
MCA bifurcation angle	-0.06 (0.05)	0.1716

Table3. The diverge of the convergence with different element sizes

	Core	Medium	Fine
Pin	691665	73052	738300
Mesh size[m]	0.0005	0.00025	0.00018
Element number	280000	1340000	2180000

Supplemental Figures and Figure Legends

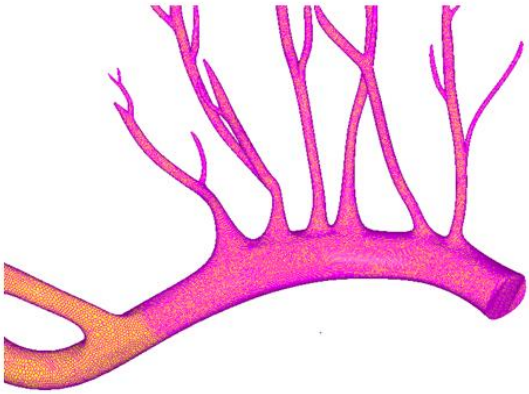

Figure 1 Numerical computational mesh model

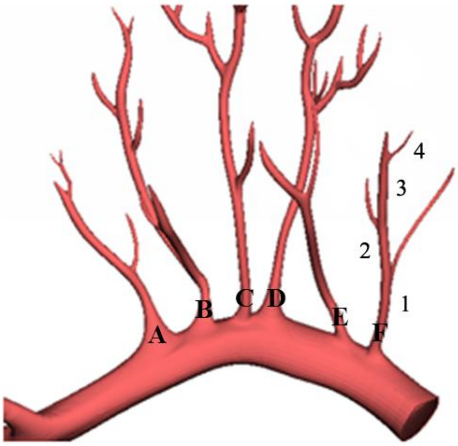

Figure 2 Geometrical characteristics of the lenticular artery.

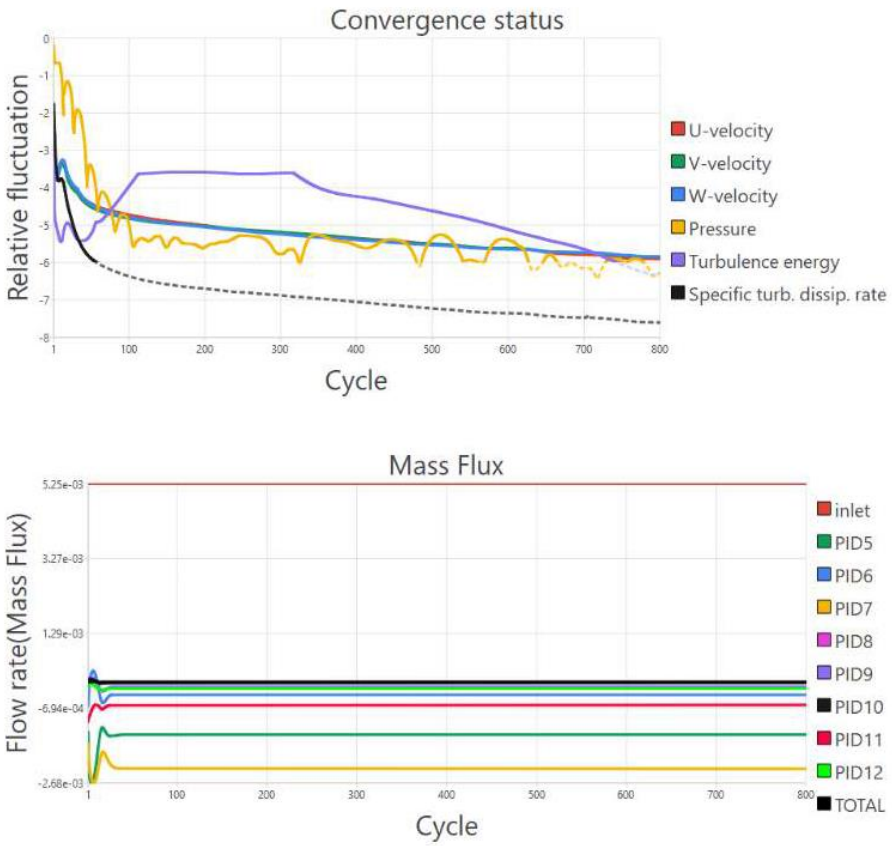

Figure 3. Convergence of the CFD simulation

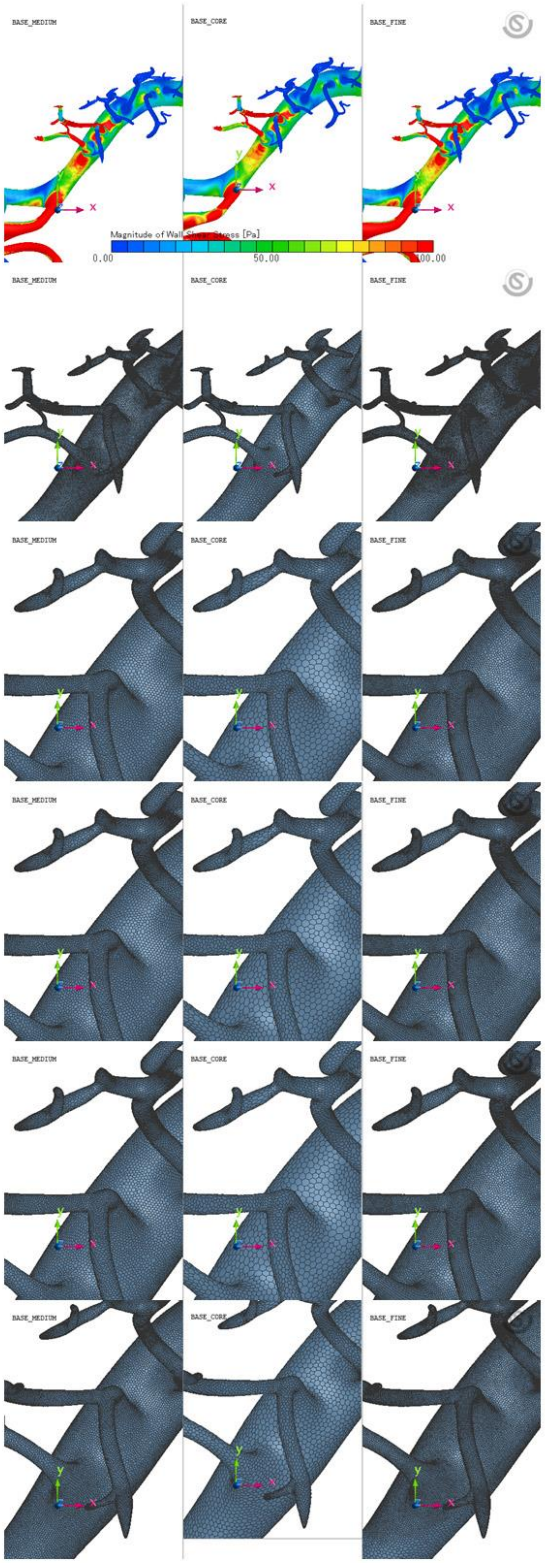

Figure 4. The simulation results with different element sizes

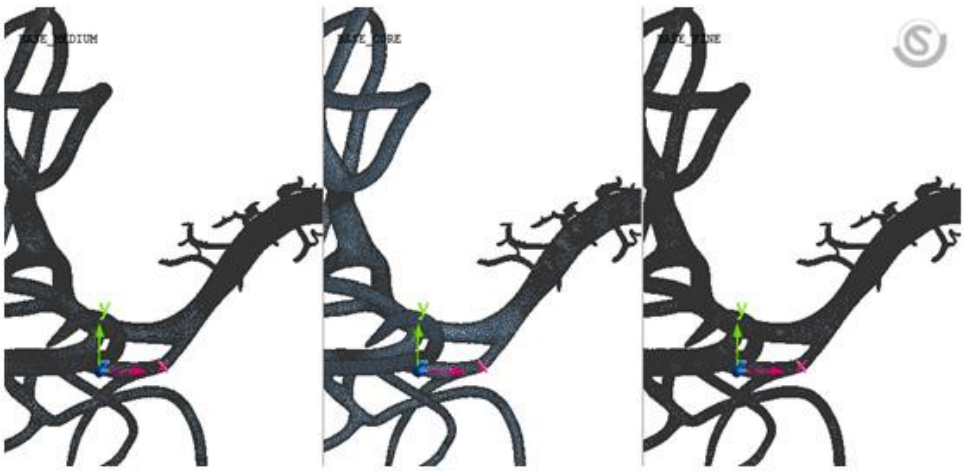

Figure 5. The mesh pattern in the boundary layer zone

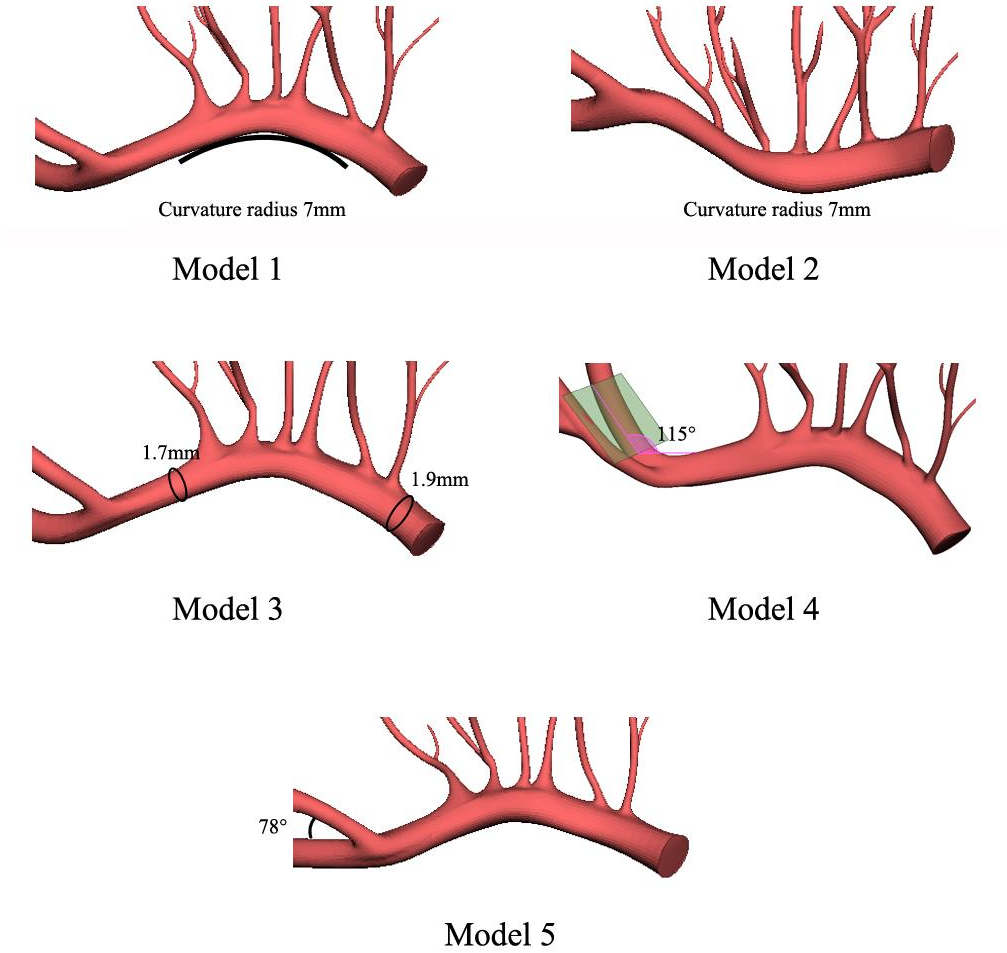

Figure 6 Reconstruction model of lesion features. Model 1: the superior-oriented M1. Model 2: the superior-oriented M1. Model 3: increased M1 segment diameter ratio (proximal/ distal). Model 4: decreased M1/M2 angle. Model 5: decreased MCA bifurcation angle.

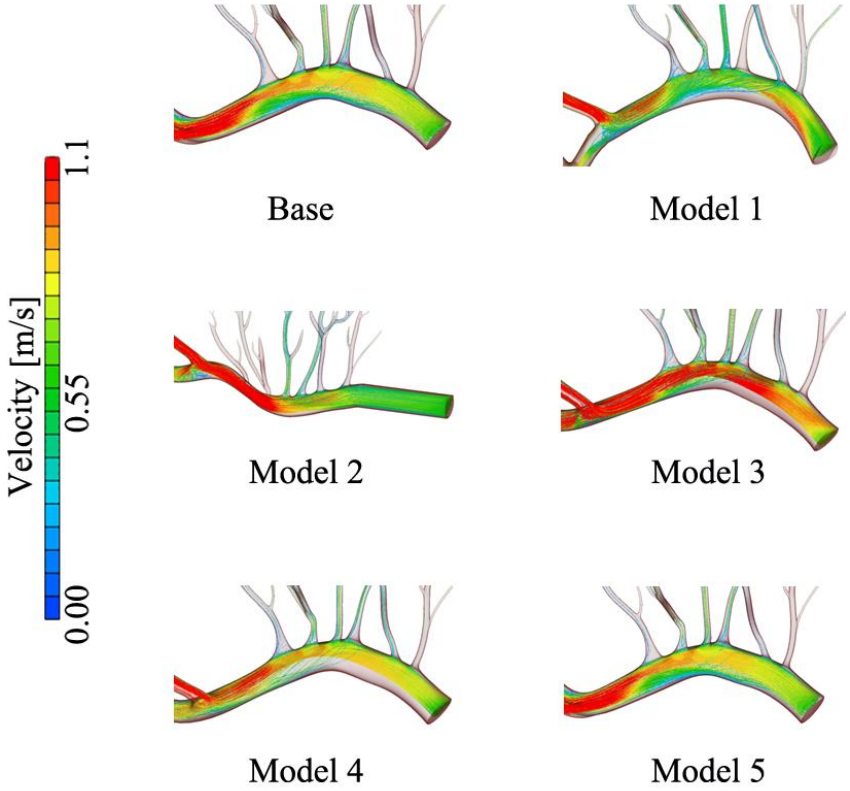

Figure 7 Blood flow chart. The blood flow in MCA and LSAs were essentially in a stable laminar flow state, and the blood flow was stable and relaxed. According to the simulation results of various models, the distal flow velocity of M1 segment was high. The M1 segment bent superior and a low-speed zone was formed in the middle of the M1 segment. In the inferior-oriented characteristic model of M1 segment, the bending curvature of M1 segment becomes smaller and the velocity increased. For the working condition of Model 3, the flow velocity in vessel increased. The decrease in the M1/M2 angle led to a decreased blood flow velocity at the distal end of M1 segment. It can be seen from the working condition of Model 5 where the change of the MCA bifurcation angle exerted no influence on the flow velocity.

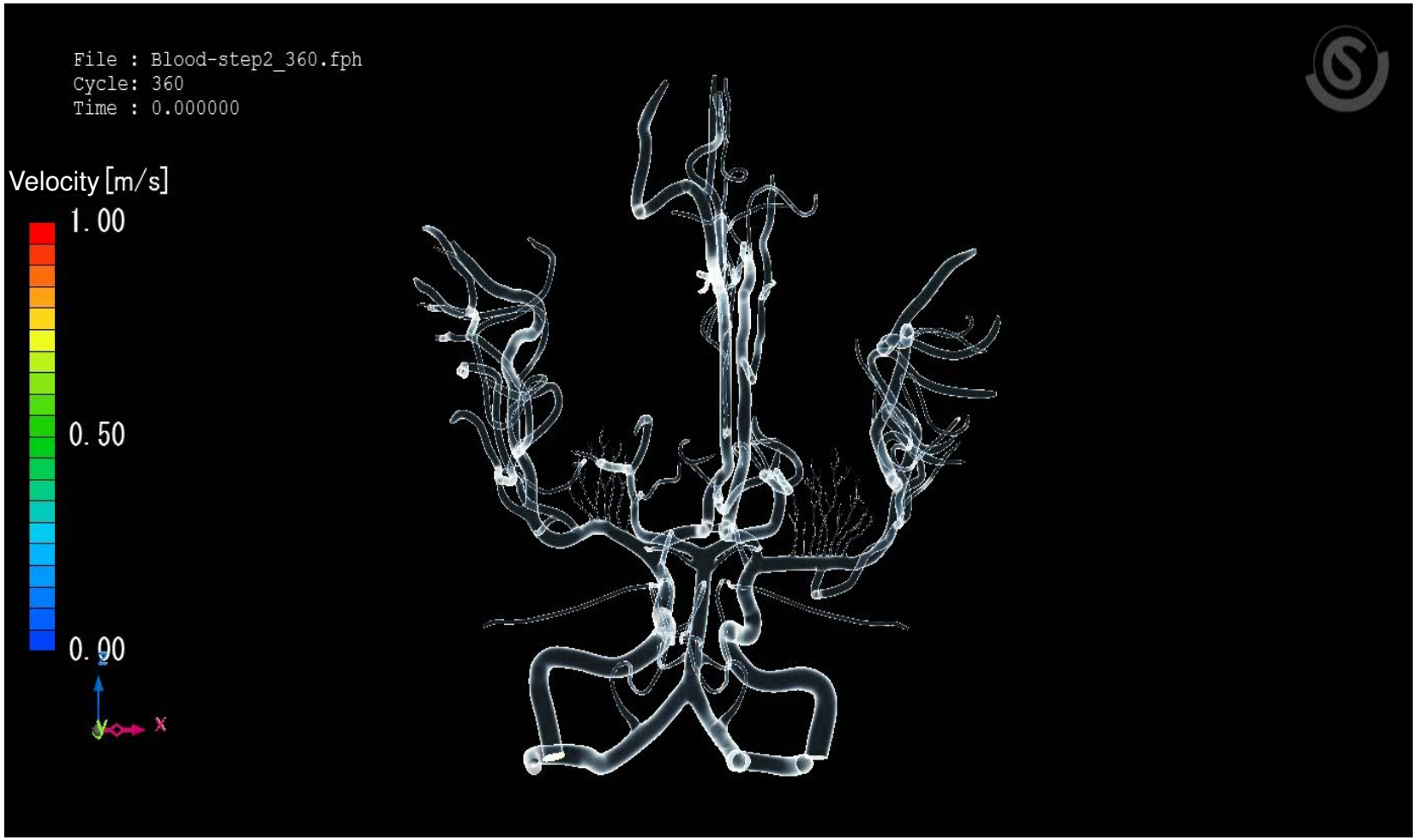

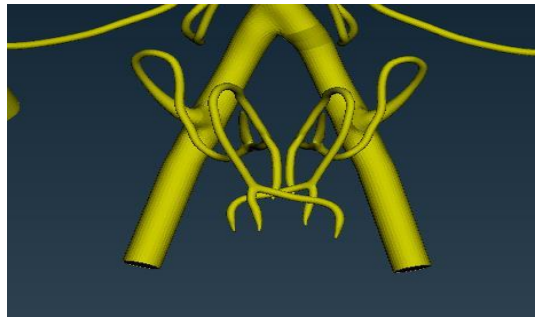

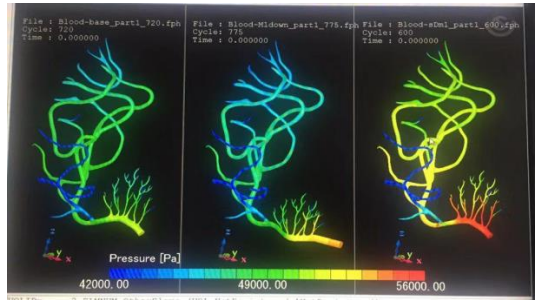

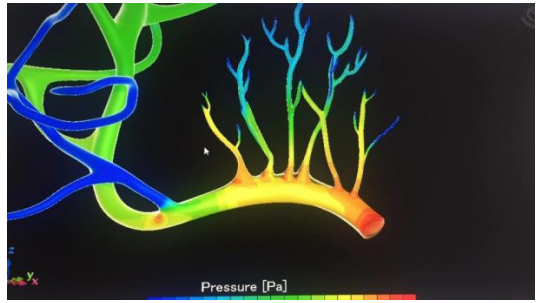

model

- Marc model (Silicon rubber vessel)
  - Analysis type Transient dynamics
  - Young's modulus 0.3 Mpa
  - Poisson's ratio 0.49
- scFLOW model (Water)
  - Analysis type Transient flow
  - Material model Incompressivle water
- Co-Simulation condition
  - Time step 0.01 sec
  - Time period 3 sec
  - Stenosis arear rate 75%model and 90% model

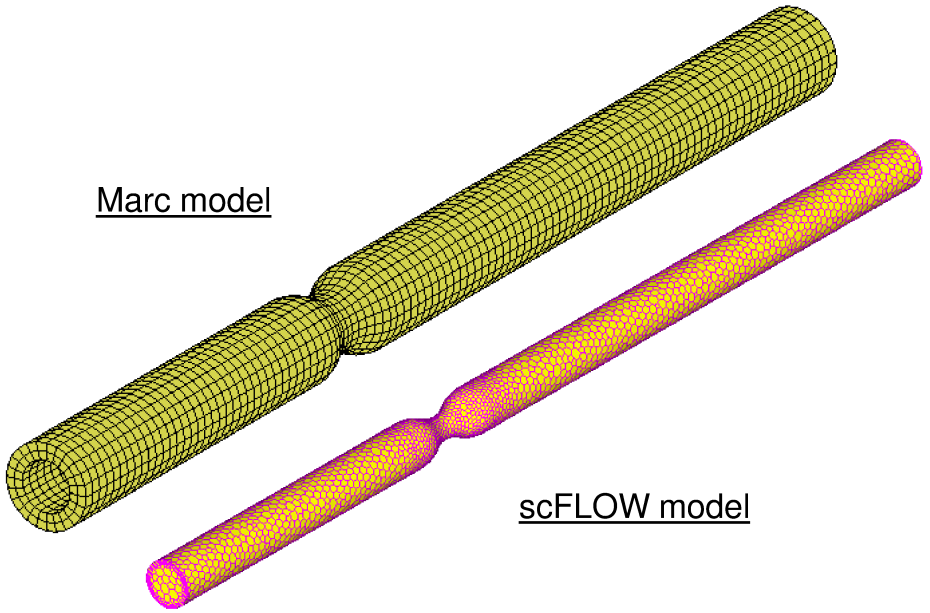

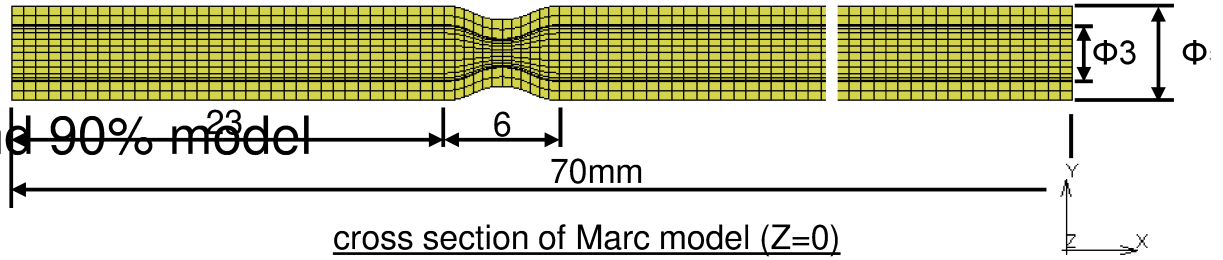

result

Stenosis rate 75%

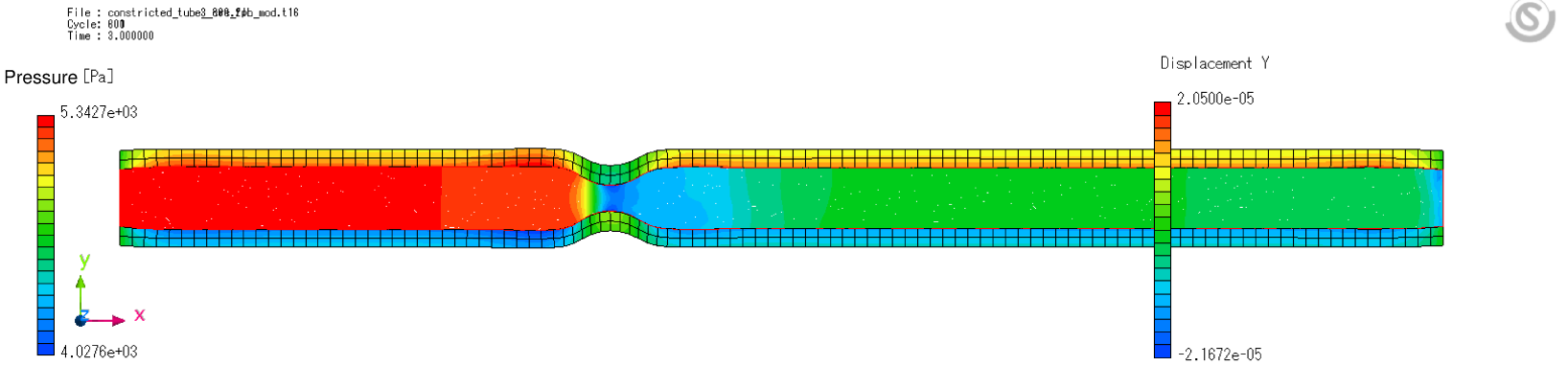

Stenosis rate 90%

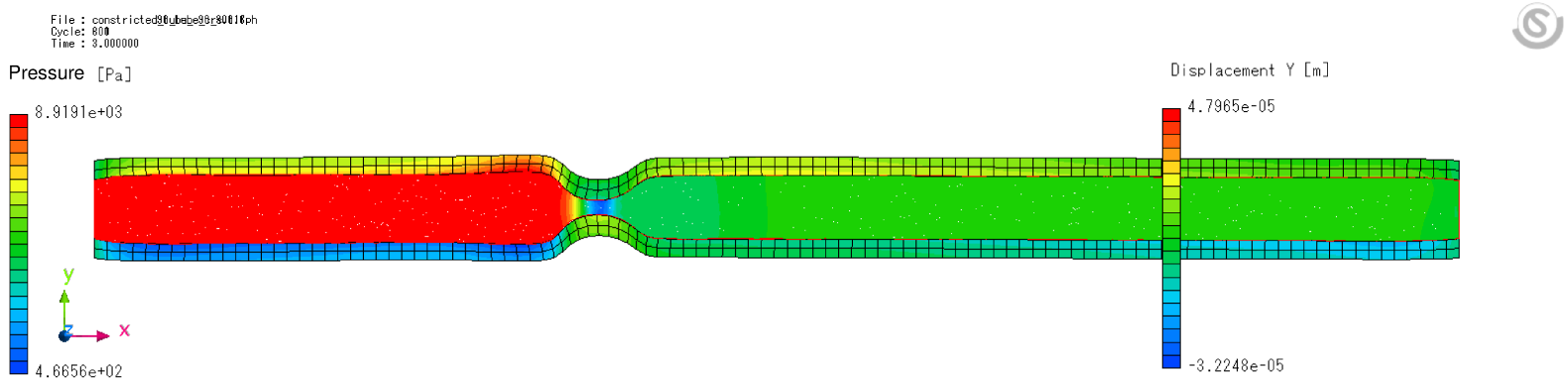

result

Stenosis rate 75%

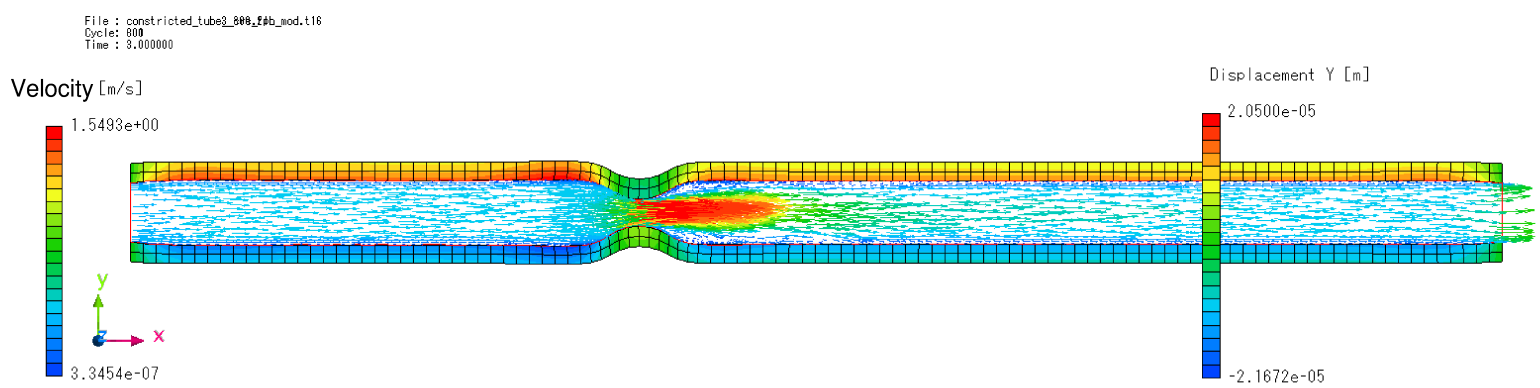

Stenosis rate 90%

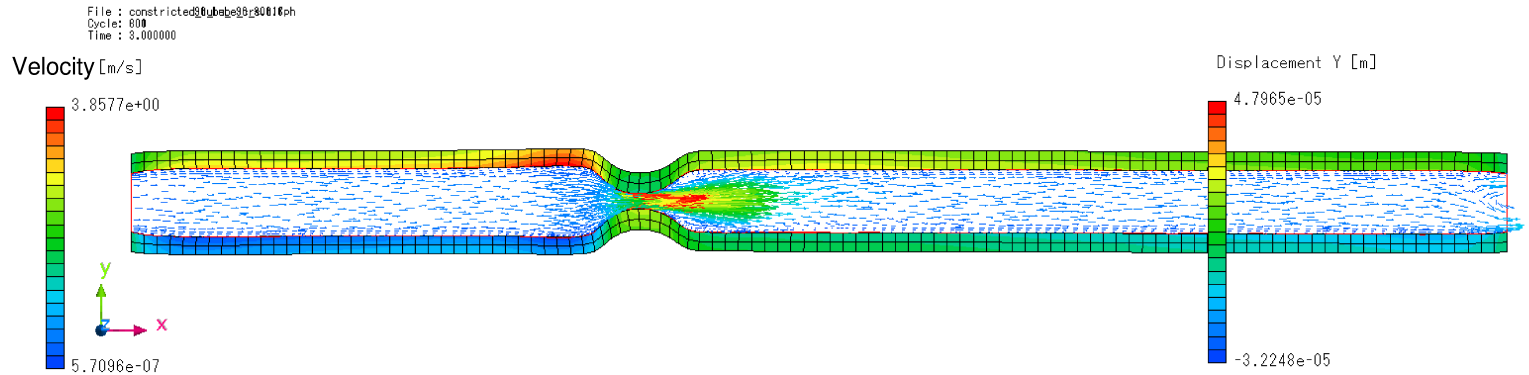

result

- Pressure history
  - Experimental result and co-simulation result comparison, 75% stenosis rate
    - Good agreement in peak pressure at inlet
      - Experimental result includes pump noise pressure turbulence

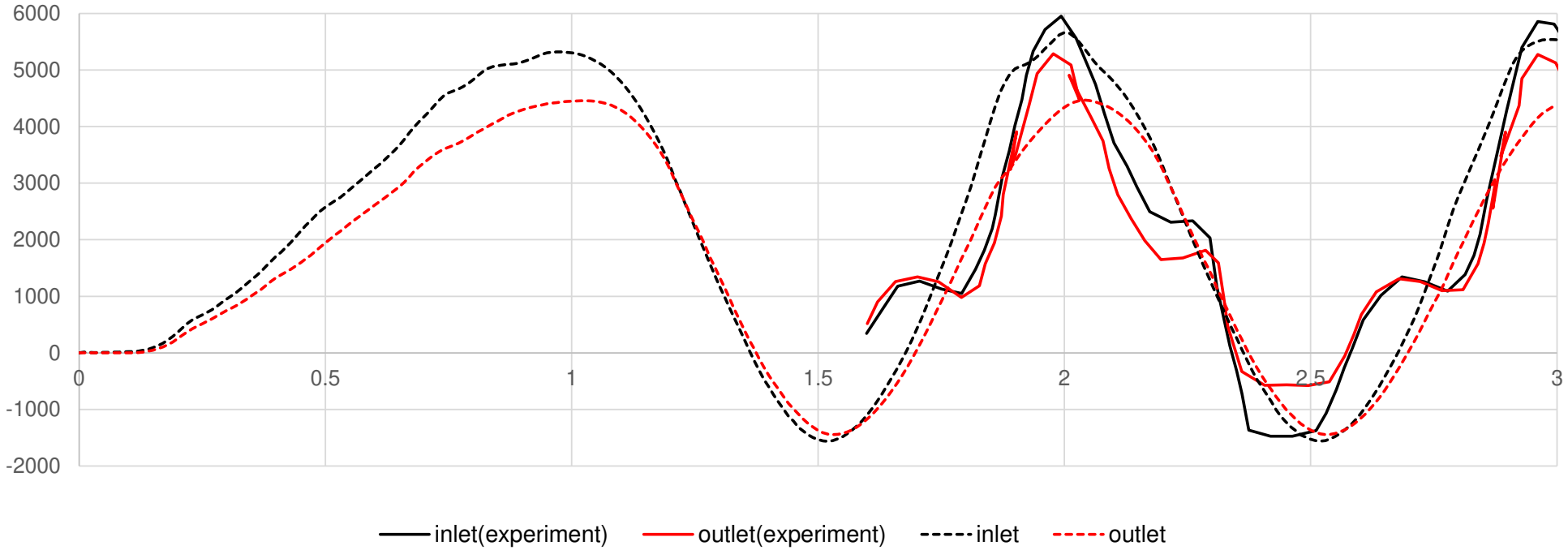

SUPPLEMENTAL MATERIAL

STROBE Statement-Checklist

	No.	Recommendation	
Title and abstract	1	(a) indicate the study's design with a commonly used term in the title or the abstract	P1L10
		(b) Provide in the abstract an informative and balanced summary of what was done and what was found	P1-2
Introduction			
Background/rationale	2	Explain the scientific background and rationale for the investigation being reported.	P3L2-P4L2
Objective	3	State specific objectives, including any prespecified hypotheses	P4L5-9
Methods			
Study design	4	Present key elements of study design early in the paper	P4L11-19
Setting	5	Describe the setting, locations, and relevant dates, including periods of recruitment, exposure, follow-up, and data collection	P4L11-19
Participants	6	*(a)* Give the eligibility criteria, and the sources and methods of selection of participants	supplemental material P4L3-11
Variables	7	Clearly define all outcomes, exposures, predictors, potential confounders, and effect modifiers. Give diagnostic criteria, if applicable	P4L11-14
Data sources/ measurement	8	For each variable of interest, give sources of data and details of methods of assessment (measurement). Describe comparability of assessment methods if there is more than one group	supplemental material P5L5-P8L13
Bias	9	Describe any efforts to address potential sources of bias	N/A
Study size	10	Explain how the study size arrived at	supplemental material P4L3-11
Quantitative variables	11	Explain how quantitative variables were handled in the analyses. If applicable, describe which grouping were chosen and why	N/A
Statistical methods	12	(*a*) Describe all statistical methods, including those used to control for confounding	supplemental material P8L15-P9L10
		(*b*) Describe any methods used to examine subgroups	N/A

		and interactions	
		(*c*) Explain how missing data were addressed	supplemental material P4L10-11
		(*d*) If applicable, describe analytical methods taking account of sampling strategy	N/A
		(*e*) Describe any sensitivity analyses	N/A
Results			
Participants	13	(*a*) Report numbers of individuals at each stage of study – e.g. numbers potentially eligible, examined for eligibility, confirmed eligible, included in the study, completing follow-up, and analysed	P5L3
		(*b*) Give reasons for non-participation at each stage	N/A
		(*c*) Consider use of a flow diagram	P4L16
Descriptive data	14	(*a*) Give characteristics of study participants (e.g. demographic, clinical, social) and information on exposures and potential confounders	P5L3-4
		(*b*) Indicate number of participants with missing data for each variable of interest	supplemental material P4L10-11
Outcome data	15*	Report numbers of outcome events or summary measures	N/A
Main results	16	(*a*) Give unadjusted estimates and, if applicable, confounder-adjusted estimates and their precision (e.g. 95% confidence interval). Make clear which confounders were adjusted for and why they were included	N/A
		(*b*) Report category boundaries when continuous variables were categorized	N/A
		(*c*) If relevant, consider translating estimats of relative risk into absolute risk for a meaningful time period	N/A
Other analyses	17	Report other analyses done – e.g. analyses of subgroups and interactions, and sensitivity analyses	N/A
Discussion			
Key results	18	Summarise key results with reference to study objectives	P9L21-P10L8
Limitation	19	Discuss limitations of the study, taking into account sources of potential bias or imprecision. Discuss both direction and magnitude of any potential bias	P13L18-P14L3
Interpretation	20	Give a cautious overall interpretation of results considering objectives, limitations, multiplicity of analyses, results from similar studies, and other relevant evidence	P11L11-P13L17

Generalisability	21	Discuss the generalisability (external validity) of the study resultes	P14L1-3
Other information			
Funding	22	Give the source of founding and the role of the founders for the present study and, if applicable, for the original study on which the present article is based	P14L13-14

Supplemental Methods

Participants

Enrolled into this study were the consecutive patients who had CT-confirmed unilateral spontaneous basal ganglia ICH (> 18 years) and had received magnetic resonance angiography (MRA)/computed tomography angiography (CTA) (within 7 days of onset) in Union Hospital, Tongji Medical College, Huazhong University of Science and Technology, Wuhan, China, between September 1, 2013 and June 30, 2019. The clinical data of the patients were collected from the institutional medical database. Those who had secondary ICH, softening range in the basal ganglia, dementia, no M1 segment, and poor imaging data were excluded. Patients whose data were missing or not available were also eliminated. The flow diagram for patient selection is shown in Figure 1. All patients' MRA/CTA images were analyzed from the ipsilateral side, with the contralateral side serving as a self-control, to study the high-risk features of ICH. The requirement for informed consent from patients was waived by the ethics committee due to the retrospective nature of the study. The data are anonymous, and all authors could only use the anonymized data for statistical analysis. STROBE was used as the reporting guideline and no extensions were used.

Neuroimaging Data

MRI was performed on a 3.0-tesla system (SIEMEHS) equipped with adequate head coils. The protocol included conventional 3-dimensional time-off light MRA, T1-weighted imaging, and T2-weighted imaging of the head. Maximum intensity projection (MIP) images were reconstructed from 3-dimensional time-off light MRA

on axial, sagittal and coronal planes in all patients. CT was performed on a 64-slice system (PHILIPS-CX). The protocol involved conventional CTA and plain CT scan of the head. MIP images were reconstructed from CTA on axial, sagittal and coronal planes in all patients.

The parameters used in our study included the MCA-related variables and other items that might be related to spontaneous basal ganglia ICH. All the parameters were measured on the Picture Archiving and Communication System. The MCA-related geometric features examined included M1 length, M1 proximal/distal diameter, shape of M1, M1 curve orientation, M1/M2 angle and MCA bifurcation angle (Figure 2A-D). M1 length and proximal/distal diameter were measured on axial plane. Shape of M1 was categorized as straight or curved based on axial and coronal MIP images of 3-dimensional time-off light MRA/CTA. We determined the orientation of the curved M1 on the basis of the direction(s) in which each M1 curve opened and measured the angle in the two directions respectively. Ventral- and dorsal-oriented M1 curves were identified by using axial MIP images, while superior- and inferior-oriented M1 curves were identified using coronal MIP images. The M1/M2 angle (the angle between M1 segment and the plane where the M2 branches were on) and MCA bifurcation angle (the angle of two M2 branches; all have two branches in our cases) were measured in different directions to fully present the relative position among the vessels. Windowing for the 3D reconstructions was validated against the multiplanar reconstructions to ensure accurate measurement.

Other parameters included the hematoma volume, and presence (or absence) of

intraventricular extension, aneurysm(s) in the adjacent vessels and stenosis of the M1 segment. The hematoma volume was measured in Picture Archiving and Communication System. The researcher manually outlined the hematoma and then the system calculated the volume automatically.

Images were analyzed twice by a researcher who was blind to all clinical information, with the two analyses being 1 month apart. To evaluate the consistency between examiners, another image reader, also blind to all clinical data, assessed 50 imaging materials randomly and independently selected from the overall imaging materials.

Control Equation of the Blood Flow in the Cerebral Vessels

Hemodynamically, the Naviers-Stokes equation, continuity equation, and motion equation of incompressible viscous fluids are commonly used to describe blood flow. The basic mechanical laws of viscous fluid flow are described, and the formulae were as follows:

(1) Naviers-Stokes equation

$$\frac{\partial v}{\partial t} + (v \bullet \Delta)v = -\frac{1}{\rho}\Delta p + \frac{\eta}{p}\Delta^2 v$$

where, v represents fluid velocity, ρ fluid density, p pressure, and η hemodynamic viscosity.

(2) Continuity equation

$$\frac{\partial u}{\partial x} + \frac{\partial v}{\partial y} + \frac{\partial w}{\partial z} = 0$$

where *u*, *v*, and *w* are the velocity components of the velocity vector on *x*, *y*, and *z*, respectively.

(3) Momentum conservation equation

$$\frac{\partial(\rho u)}{\partial t}+div(\rho uU)=div(\eta gradu)+Su-\frac{\partial p}{\partial x}$$
$$\frac{\partial(\rho v)}{\partial t}+div(\rho vU)=div(\eta gradv)+Sv-\frac{\partial p}{\partial y}$$
$$\frac{\partial(\rho w)}{\partial t}+div(\rho wU)=div(\eta gradw)+Sw-\frac{\partial p}{\partial z}$$

where, *u*, *v,* and *w* are the velocity components of the velocity vector on *x*, *y,* and *z*, respectively, and η is the dynamic viscosity of the fluid; *Su*, *Sv,* and *Sw* are the broad source terms of the three momentum conservation equations, respectively.

(4) Fluid properties

In the study, blood was seen as an incompressible Newtonian fluid, with blood density ρ=1050 kg/m^3 and viscosity=0.0024 Pa·s (in ref 10, the viscosity was set at 0.0035, being virtually identical to the parameter used in the present paper). This study ignored the influence of gravity in the simulation, and the vascular wall was taken as a non-viscoelastic rigid wall under the condition of no slip referring to the previous studies. [1-3] The inner diameter at the entrance of M1 segment was within 2.1~2.7 mm. We enrolled 158 patients, the peak blood velocity in the brain was 0.4~1.1 m/s, and the peak Re of Re=$\rho vD/\mu$ number was 367~1300. Therefore, in the numerical simulation, the blood movement in the cerebral artery was assumed to be a steady laminar flow, and the inlet flow rate was defined as 5e-6 m^3/*s*.

(5) Geometric model, mesh and boundary conditions

In the analysis with the scFLOW module from MSC Cradle, the grid was first divided based on the scFLOW Preprocessor software. Due to the irregularity and complexity of the model, the unstructured octree method was adopted to divide it, and the grid was of polyhedral type. The meshes were divided into intelligent meshes, i.e., when the geometric shapes change, the meshes divided automatically and reasonably according to the geometric shapes encountered, so as to obtain a relatively optimal mesh cell. For MCA meshing, non-equidistant meshing along the radius direction was adopted to improve the calculation accuracy of the boundary layer of the pipe wall, while for all LSAs, non-equidistant meshing was used and local refinement was performed at each bifurcation point to improve the accuracy. There were roughly 1.35 million units in the model (supplementary Figure 1), and the convergence is also provided and discussed in this paper. Furthermore, the mesh data including the boundary layer zone, are also detailed in supplementary Figure 5.

Statistical analysis

Statistical analysis was performed by employing Statistical Product and Service Solutions 12.0 for Windows. For descriptive analysis, frequency and percentage were used for independent variables. The paired *t*-test was employed to compare quantitative data of the MCA geometric features. The Bowker test was utilized to compare enumeration data of the MCA geometric features. Then, multivariate logistic regression analysis was conducted to identify the association between the MCA geometric features and hematoma volume. Variables input into the model included age, gender, smoking and drinking habits, hypertension, diabetes mellitus,

hypercholesterolemia, coronary artery disease, previous ischemic stroke, previous ICH, time of scanning, intraventricular extension and the geometric features of MCA. The relationship between the MCA geometric features and NIHSS score was also examined by multivariate logistic regression. Variables input into the model were age, gender, smoking and drinking habits, hypertension, diabetes mellitus, hypercholesterolemia, coronary artery disease, previous ischemic stroke, previous ICH, time of scanning, intraventricular extension, hematoma volume and the MCA geometric features. Adjusted odds ratios (ORs) and 95% confidence intervals (CIs) for variables were obtained. For all analyses, differences were tested using two-tailed tests, and a $P<0.05$ was considered to be statistically significant.

Supplemental references

1. Leng X, Lan L, Ip HL, et al. Hemodynamics and stroke risk in intracranial atherosclerotic disease. Ann Neurol. 2019 May;85(5):752-764.
2. Leng X, Scalzo F, Ip HL, et al. Computational fluid dynamics modeling of symptomatic intracranial atherosclerosis may predict risk of stroke recurrence. PLoS One. 2014 May 12;9(5):e97531.
3. Liu J, Yan Z, Pu Y, et al. Functional assessment of cerebral artery stenosis: a pilot study based on computational fluid dynamics. J Cereb Blood Flow Metab. 2017 Jul;37(7):2567-2576.

Supplemental Tables

Table 1 shows determinants associated with hematoma volume. Patients who had suffered hypertension had larger hematoma volume (β=9.83, SE=4.93, *P*=0.0492), while patients who had intraventricular extension had smaller hematoma volume (β=-13.22, SE=3.80, P=0.0008). Other covariates, including MCA geometric features, showed no significant differences in multivariable linear regression analysis.

Covariate	**Intracerebral Hemorrhage Volume**	
	β (SE)	***P* Value**
Age	-0.18 (0.17)	0.3143
Gender	-1.11 (4.45)	0.8045
Smoking	-0.27 (4.60)	0.9539
Drinking	-1.58 (4.40)	0.7208
Hypertension	9.83 (4.93)	0.0492
Diabetes mellitus	6.81 (7.44)	0.3625
Hypercholesterolemia	0.97 (5.21)	0.8523
Coronary artery disease	-6.96 (9.21)	0.4519
Previous ischemic stroke	7.77 (7.52)	0.3044
Previous ICH	15.88 (10.78)	0.1444
Time to scan	0.14 (0.11)	0.2153
Intraventricular extension	-13.22 (3.80)	0.0008
M1 length	0.42 (0.30)	0.1572
M1 diameter ratio (proximal/ distal)	-14.54 (8.85)	0.1041

M1 shape and curve orientation (axial)	-3.45 (6.46)	0.5952
Bending angle (axial)	0.01 (0.18)	0.9347
M1 shape and curve orientation (coronal)	-2.16 (6.61)	0.7446
Bending angle (coronal)	0.16 (0.09)	0.0886
M1/M2 angle	0.02 (0.08)	0.8276
MCA bifurcation angle	-0.06 (0.07)	0.4325

Table 2 shows determinants associated with NIHSS score. Predictors of NIHSS score identified through multivariable linear regression analysis were age and hematoma volume. The older patients (β=0.27, SE=0.11, *P*=0.0161) and those who had larger hematoma volume (β=0.26, SE=0.06, *P*=0.0002) had higher NIHSS score. Other covariates, including MCA geometric features, were not associated with NIHSS score.

Covariate	**NIHSS score**	
	β (SE)	***P* Value**
Age	0.27 (0.11)	0.0161
Gender	2.29 (2.87)	0.4269
Smoking	1.97 (2.72)	0.4721
Drinking	-0.60 (2.72)	0.8278
Hypertension	0.80 (3.20)	0.8023
Diabetes mellitus	4.67 (4.69)	0.3241
Hypercholesterolemia	2.85 (3.07)	0.3570
Coronary artery disease	-3.72 (5.90)	0.5312
Previous ischemic stroke	4.01 (5.13)	0.4380
Previous ICH	2.72 (11.47)	0.8133
Time to scan	0.09 (0.21)	0.6527
Intraventricular extension	-4.72 (2.39)	0.0528
Hematoma volume	0.26 (0.06)	0.0002
M1 segment length	-0.16 (0.21)	0.4485

M1 segment diameter ratio (proximal/ distal)	3.76 (5.39)	0.4886
M1 segment shape and curve orientation (axial)	2.88 (4.04)	0.4785
Bending angle (axial)	-0.07 (0.12)	0.5756
M1 segment shape and curve orientation (coronal)	1.62 (3.74)	0.6659
Bending angle (coronal)	0.08 (0.06)	0.2090
M1/M2 angle	-0.03 (0.05)	0.5760
MCA bifurcation angle	-0.06 (0.05)	0.1716

Table3. The diverge of the convergence with different element sizes

	Core	Medium	Fine
Pin	691665	73052	738300
Mesh size[m]	0.0005	0.00025	0.00018
Element number	280000	1340000	2180000

Supplemental Figures and Figure Legends

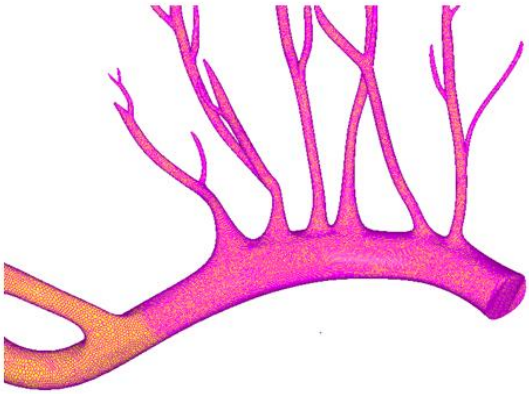

Figure 1 Numerical computational mesh model

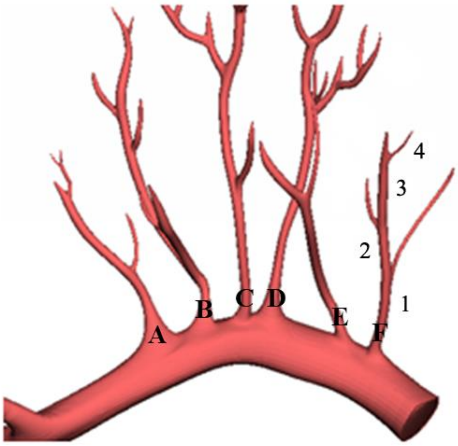

Figure 2 Geometrical characteristics of the lenticular artery.

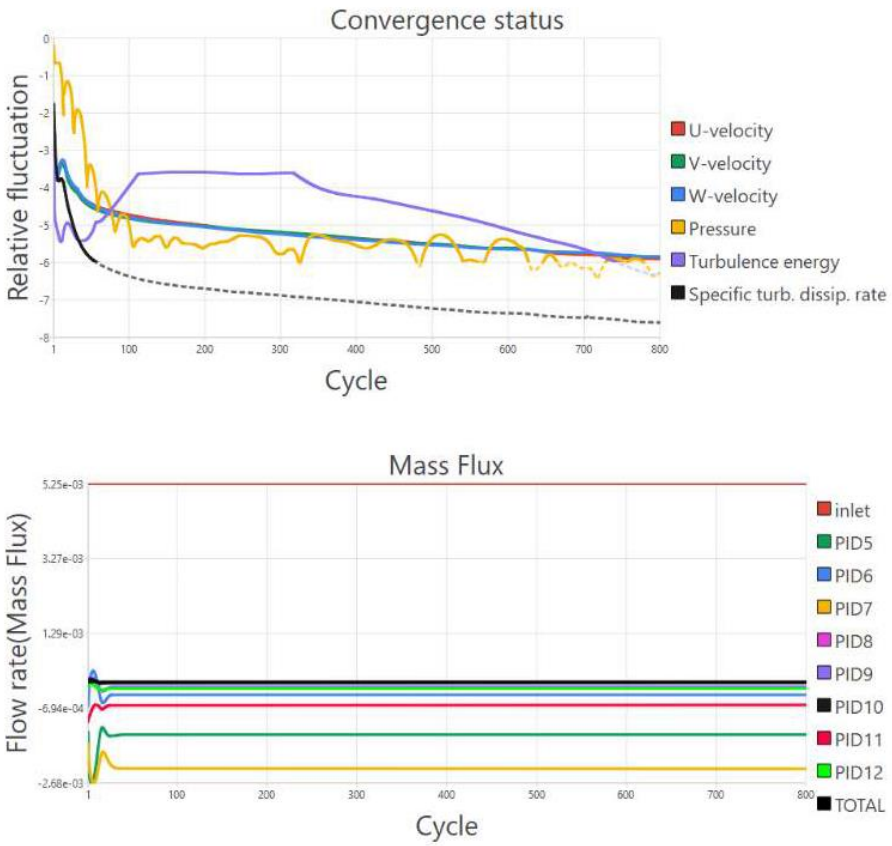

Figure 3. Convergence of the CFD simulation

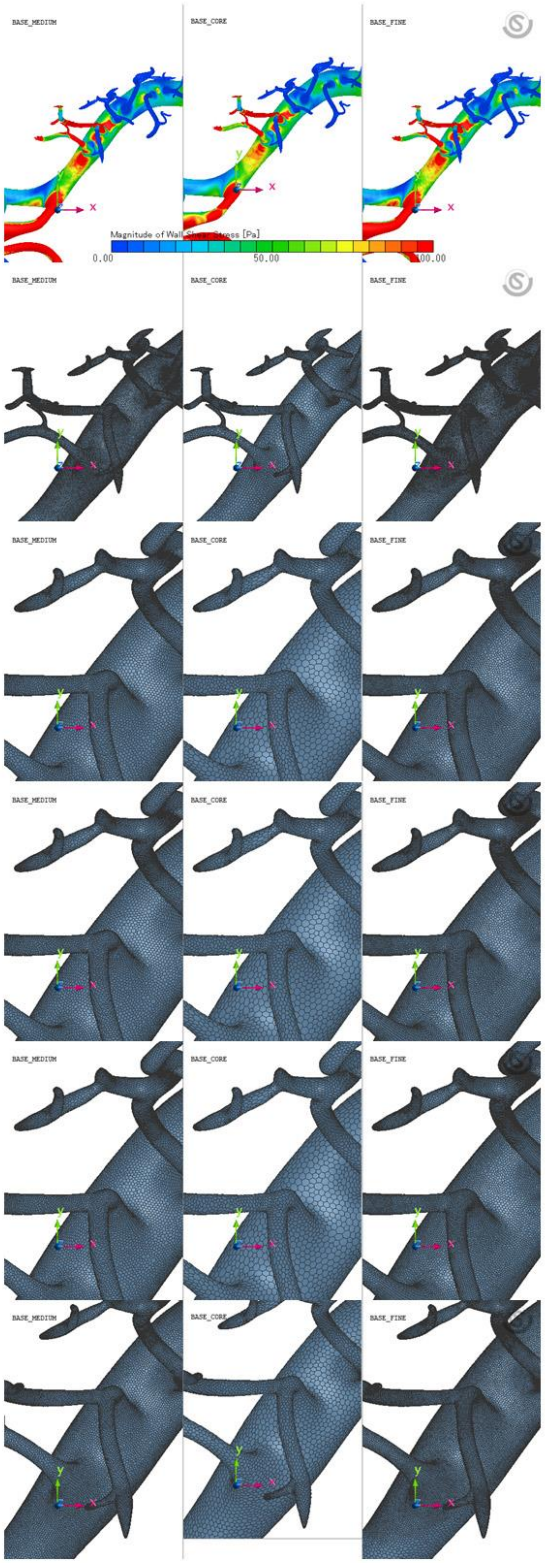

Figure 4. The simulation results with different element sizes

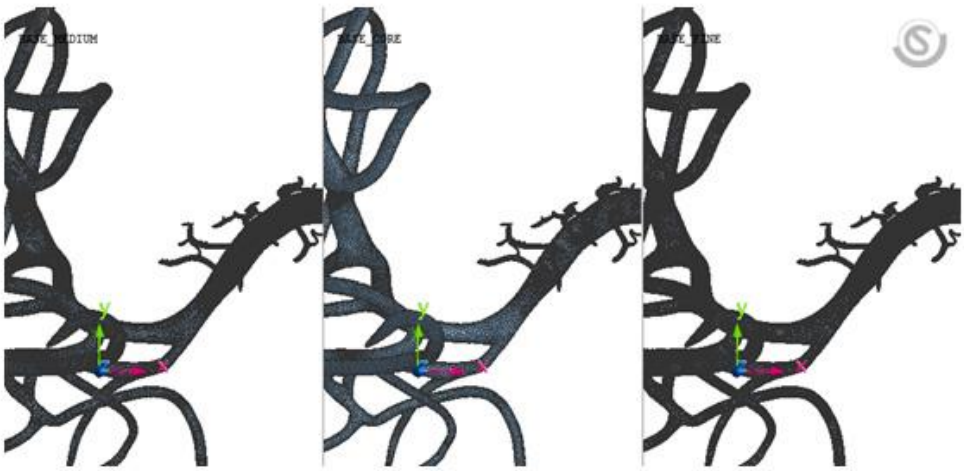

Figure 5. The mesh pattern in the boundary layer zone

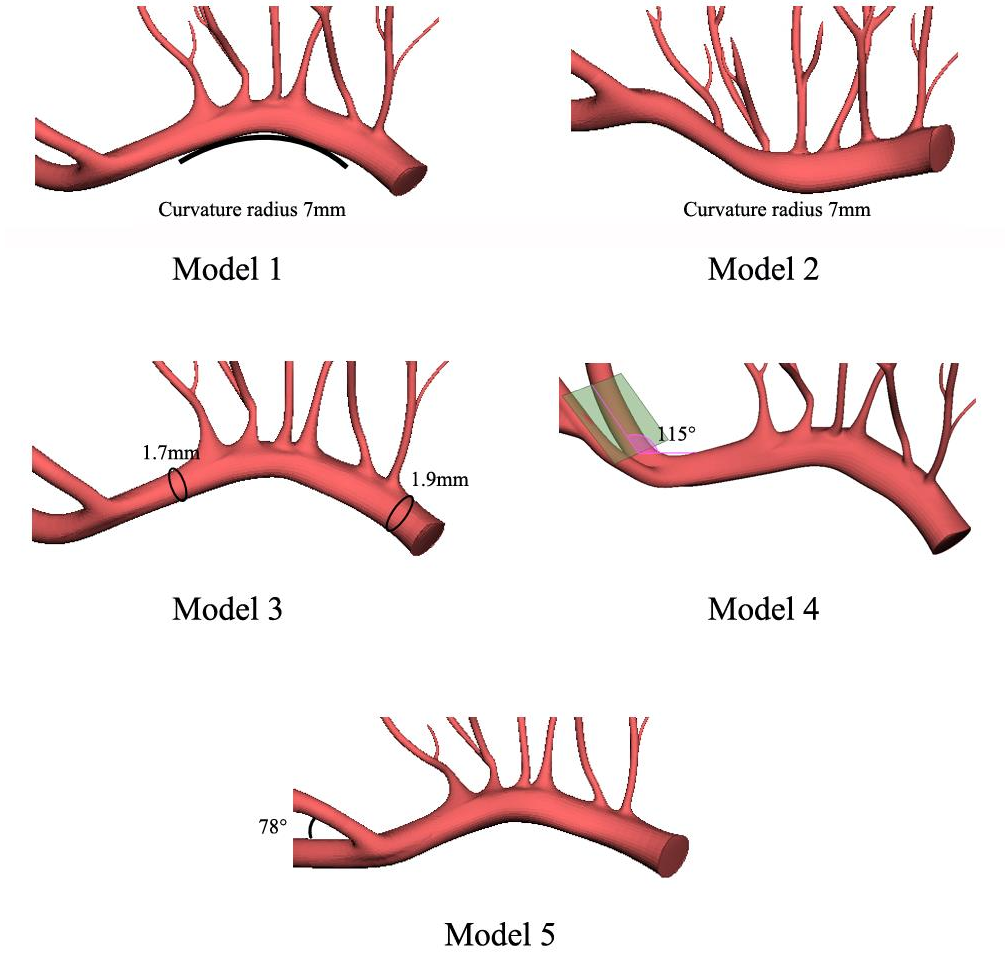

Figure 6 Reconstruction model of lesion features. Model 1: the superior-oriented M1. Model 2: the superior-oriented M1. Model 3: increased M1 segment diameter ratio (proximal/ distal). Model 4: decreased M1/M2 angle. Model 5: decreased MCA bifurcation angle.

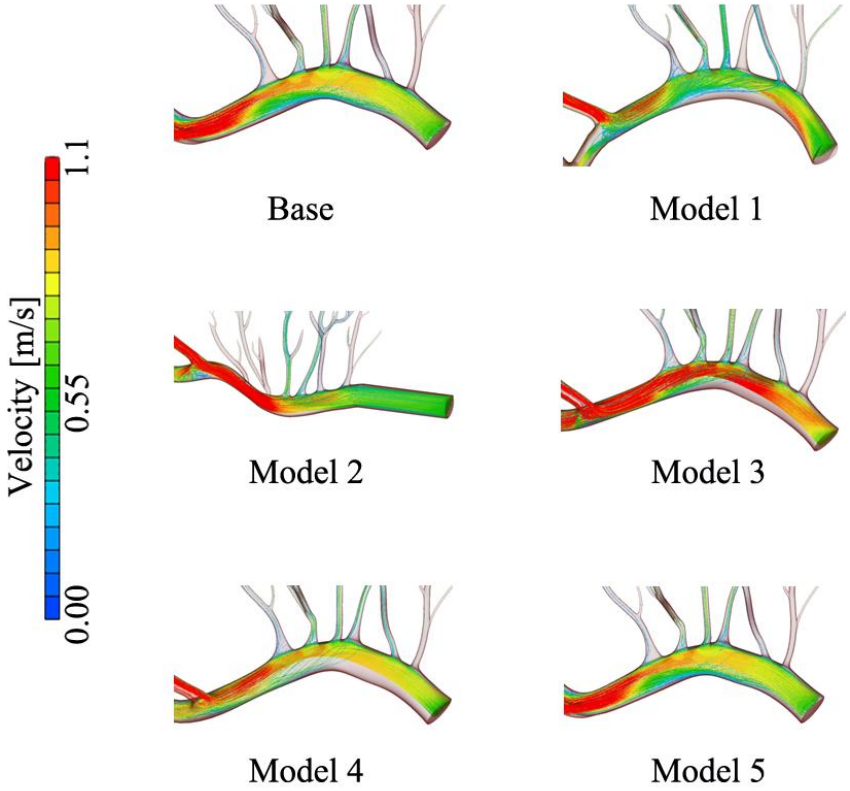

Figure 7 Blood flow chart. The blood flow in MCA and LSAs were essentially in a stable laminar flow state, and the blood flow was stable and relaxed. According to the simulation results of various models, the distal flow velocity of M1 segment was high. The M1 segment bent superior and a low-speed zone was formed in the middle of the M1 segment. In the inferior-oriented characteristic model of M1 segment, the bending curvature of M1 segment becomes smaller and the velocity increased. For the working condition of Model 3, the flow velocity in vessel increased. The decrease in the M1/M2 angle led to a decreased blood flow velocity at the distal end of M1 segment. It can be seen from the working condition of Model 5 where the change of the MCA bifurcation angle exerted no influence on the flow velocity.

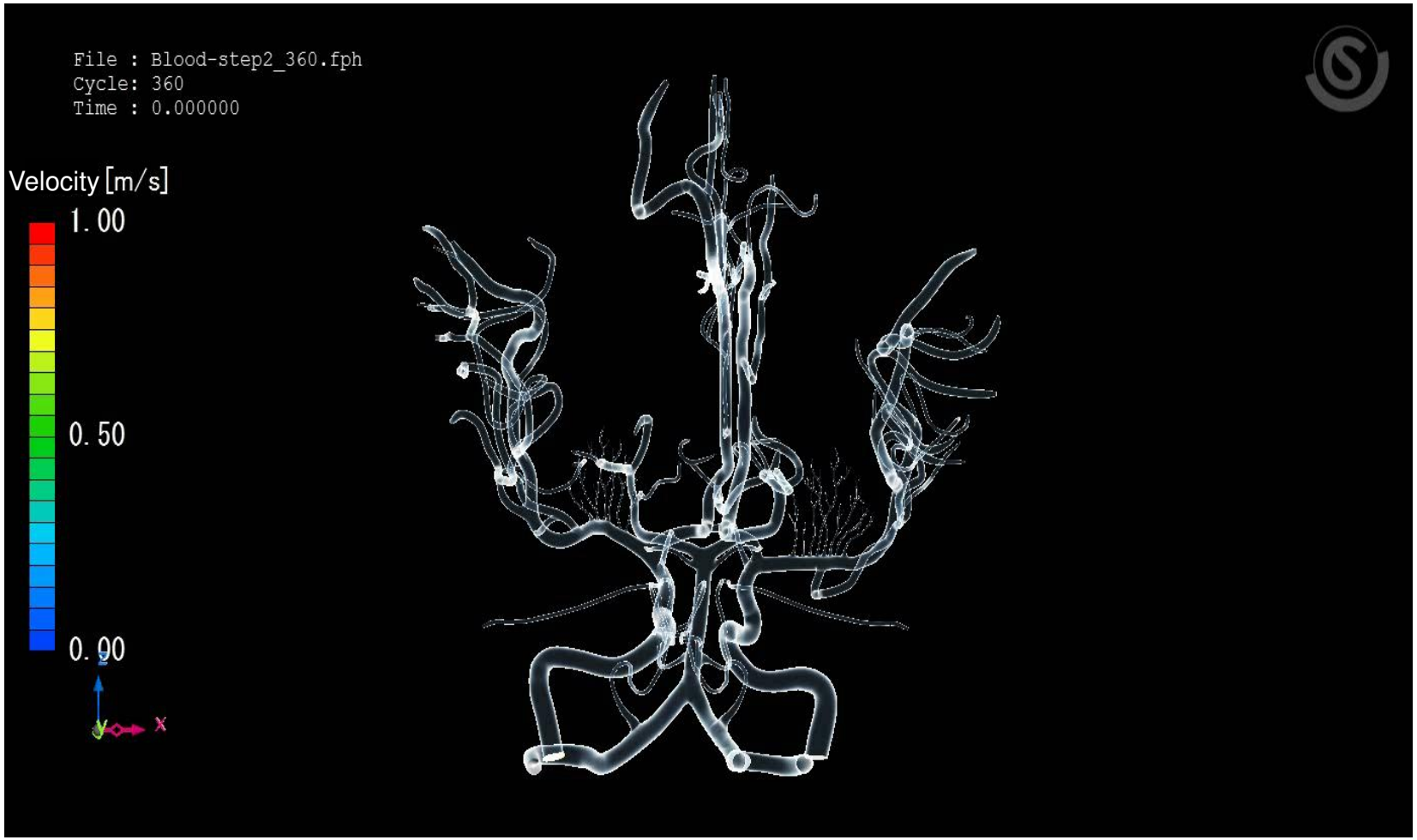

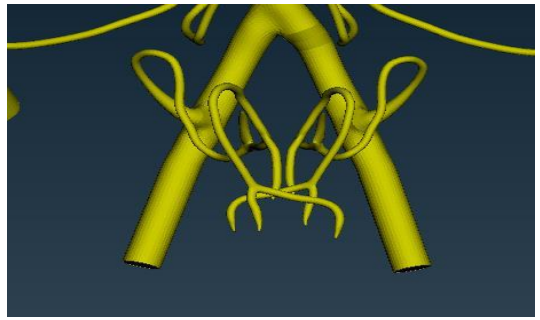

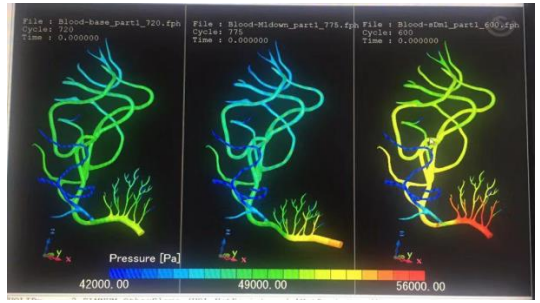

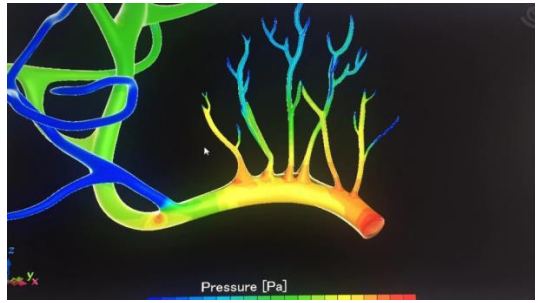

model

- Marc model (Silicon rubber vessel)
  - Analysis type Transient dynamics
  - Young's modulus 0.3 Mpa
  - Poisson's ratio 0.49
- scFLOW model (Water)
  - Analysis type Transient flow
  - Material model Incompressivle water
- Co-Simulation condition
  - Time step 0.01 sec
  - Time period 3 sec
  - Stenosis arear rate 75%model and 90% model

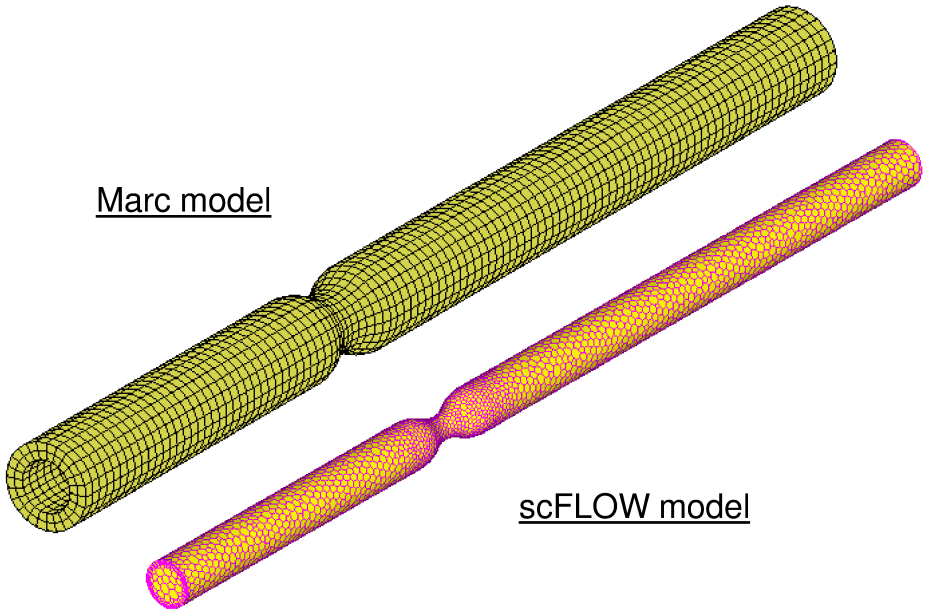

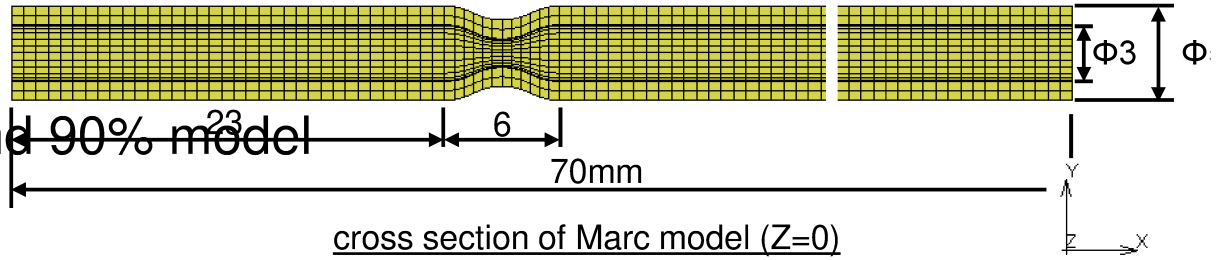

result

Stenosis rate 75%

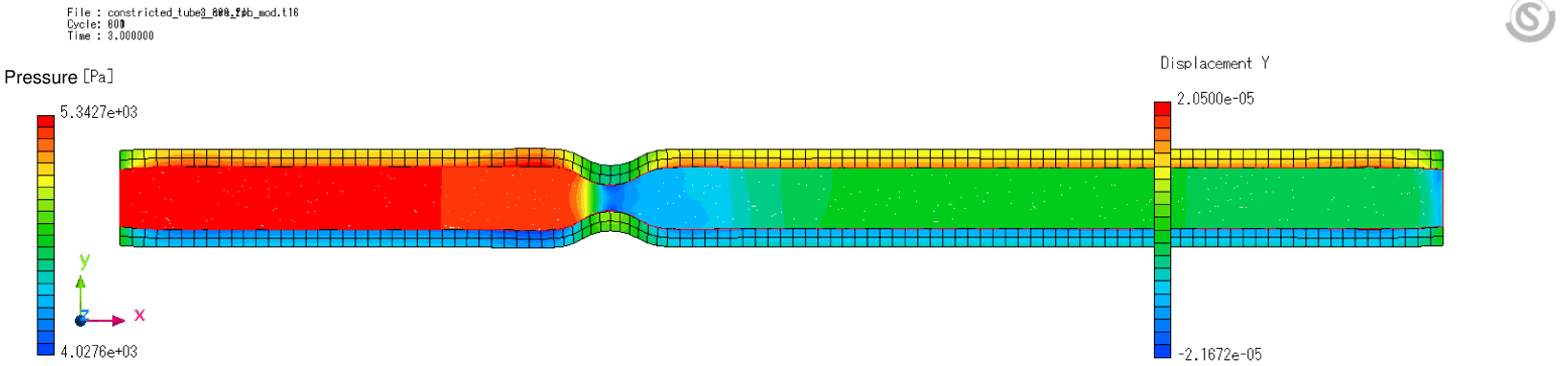

Stenosis rate 90%

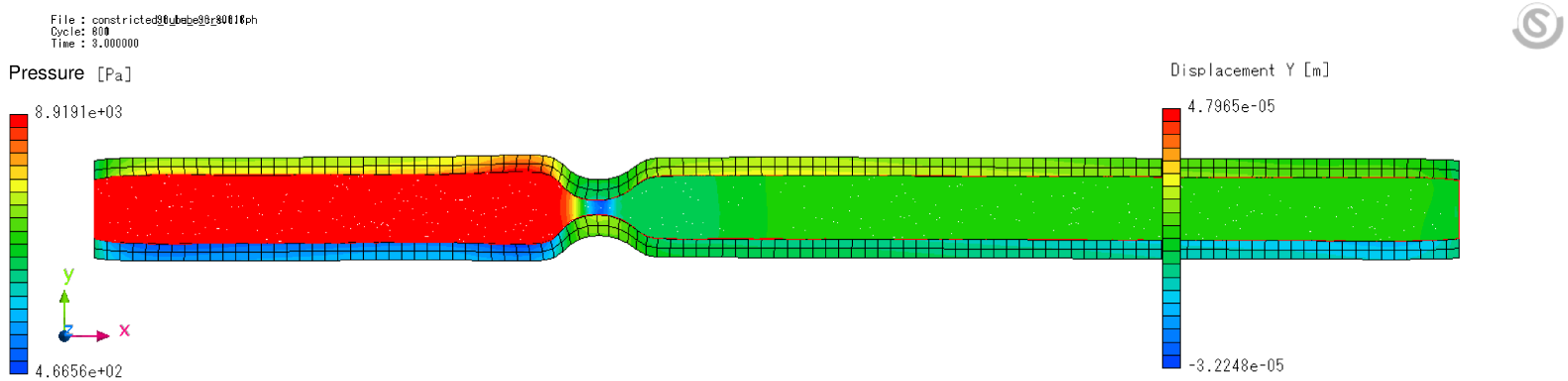

result

Stenosis rate 75%

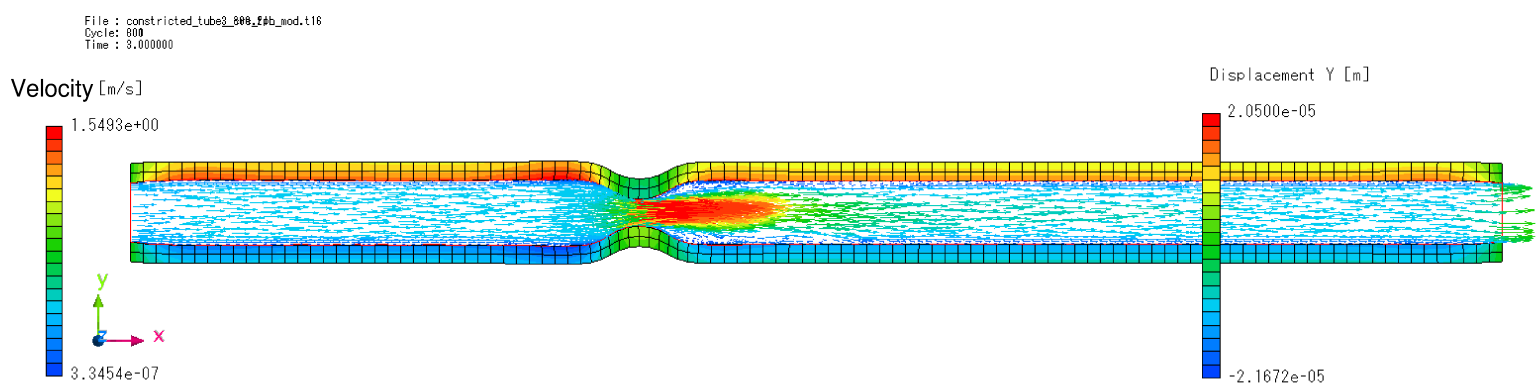

Stenosis rate 90%

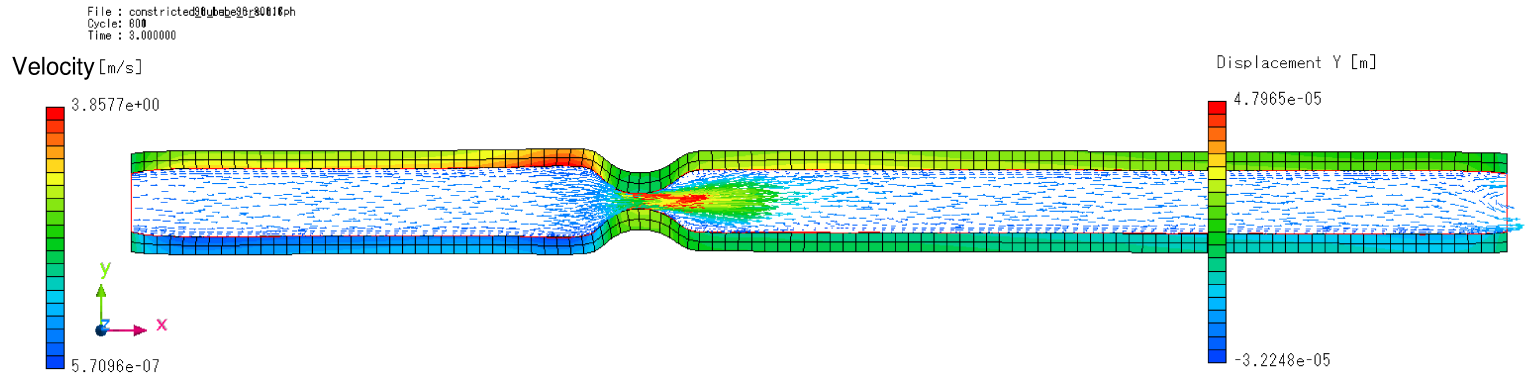

result

- Pressure history
  - Experimental result and co-simulation result comparison, 75% stenosis rate
    - Good agreement in peak pressure at inlet
      - Experimental result includes pump noise pressure turbulence